HHS Public Access

Author manuscript

Nat Cell Biol. Author manuscript; available in PMC 2024 July 09.

Published in final edited form as:

Nat Cell Biol. 2023 August ; 25(8): 1208–1222. doi:10.1038/s41556-023-01185-x.

STING is a cell-intrinsic metabolic checkpoint restricting aerobic glycolysis by targeting HK2

Liting Zhang[1,2,3,4,10], **Congqing Jiang**[5,10], **Yunhong Zhong**[1,2], **Kongliang Sun**[5], **Huiru Jing**[2,6], **Jiayu Song**[2,6], **Jun Xie**[1,2], **Yaru Zhou**[1,2], **Mao Tian**[7], **Chuchu Zhang**[1,2], **Xiaona Sun**[1,2], **Shaowei Wang**[1,2], **Xi Cheng**[1,2], **Yuelan Zhang**[2,6], **Wei Wei**[8,9], **Xiang Li**[6,8,9], **Bishi Fu**[2,6], **Pinghui Feng**[7], **Bing Wu**[2,6], **Hong-Bing Shu**[2,6], **Junjie Zhang**[1,2,3,4]

[1]The State Key Laboratory Breeding Base of Basic Science of Stomatology & Key Laboratory of Oral Biomedicine Ministry of Education, School & Hospital of Stomatology, State Key Laboratory of Virology, Medical Research Institute, Wuhan University, Wuhan, China.

[2]Frontier Science Center for Immunology and Metabolism, Wuhan University, Wuhan, China.

[3]Department of Pulmonary and Critical Care Medicine, Zhongnan Hospital of Wuhan University, Wuhan, China.

[4]Wuhan Research Center for Infectious Diseases and Cancer, Chinese Academy of Medical Sciences, Wuhan, China.

[5]Department of Colorectal and Anal Surgery, Zhongnan Hospital of Wuhan University, Wuhan, China.

[6]Medical Research Institute, Wuhan University, Wuhan, China.

[7]Section of Infection and Immunity, Herman Ostrow School of Dentistry, Norris Comprehensive Cancer Center, University of Southern California, Los Angeles, CA, USA.

[8]Department of Neurosurgery, Zhongnan Hospital, Wuhan University, Wuhan, China.

[9]Brain Research Center, Zhongnan Hospital, Wuhan University, Wuhan, China.

[10]These authors contributed equally: Liting Zhang, Congqing Jiang.

Abstract

Correspondence and requests for materials should be addressed to Junjie Zhang. junjiezhang@whu.edu.cn.

Author contributions

L.Z., P.F., B.W., H.-B.S. and J.Z. designed and supervised the study. L.Z., Y. Zhong, H.J., J.S. Y. Zhou and C.Z. performed most of the experiments. Y. Zhang and B.F. performed the IP–MS study. J.X. and M.T. analysed the sequencing and metabolomics data. K.S., X.S., S.W., X.C., W.W. and X.L. helped with animal experiments. C.J. and K.S. collected patient samples and helped with the related analysis. L.Z. and J.Z. wrote the paper. All of the authors approved the manuscript.

Competing interests

The authors declare no competing interests.

Additional information

Extended data is available for this paper at https://doi.org/10.1038/s41556-023-01185-x.

Supplementary information The online version contains supplementary material available at https://doi.org/10.1038/s41556-023-01185-x.

Evasion of antitumour immunity is a hallmark of cancer. STING, a putative innate immune signalling adaptor, has a pivotal role in mounting antitumour immunity by coordinating innate sensing and adaptive immune surveillance in myeloid cells. STING is markedly silenced in various human malignancies and acts as a cell-intrinsic tumour suppressor. How STING exerts intrinsic antitumour activity remains unclear. Here, we report that STING restricts aerobic glycolysis independent of its innate immune function. Mechanistically, STING targets hexokinase II (HK2) to block its hexokinase activity. As such, STING inhibits HK2 to restrict tumour aerobic glycolysis and promote antitumour immunity in vivo. In human colorectal carcinoma samples, lactate, which can be used as a surrogate for aerobic glycolysis, is negatively correlated with STING expression level and antitumour immunity. Taken together, this study reveals that STING functions as a cell-intrinsic metabolic checkpoint that restricts aerobic glycolysis to promote antitumour immunity. These findings have important implications for the development of STING-based therapeutic modalities to improve antitumour immunotherapy.

STING in antigen-presenting cells has an important role in coordinating innate immune sensing and the subsequent activation of antitumour adaptive immune surveillance[1–5]. After sensing double-stranded DNA (dsDNA), the DNA sensor cyclic GMP–AMP synthase (cGAS) produces cGAMP[6,7], which binds to and activates STING (encoded by *STING1*, also known as MITA)[8,9], an endoplasmic reticulum (ER)-localized transmembrane adaptor protein. STING recruits and activates TANK-binding kinase 1 (TBK1), which in turn phosphorylates and activates interferon regulatory factor 3 (IRF3) to drive the expression of type I interferons (IFNs) and chemokines[4,5]. The STING-dependent innate immune sensing pathway is required to initiate T-cell-dependent antitumour immune responses[2,10]. However, our understanding of the cell-intrinsic role of STING remains very limited.

Accumulating evidence indicates that STING possesses cell-intrinsic tumour suppressive activity. Cancer cells contain cytosolic dsDNA due to genome instability or mitochondrial dysfunction, which would lead to the activation of STING-mediated antitumour immunity and tumour rejection if left unmanipulated. To deal with this issue, STING is epigenetically silenced in various cancer types[11–16]. Accordingly, efforts have been taken to restore STING expression to improve cancer therapy[11,13,14]. The current theme is that type I IFN responses generated by STING restoration in tumour cells facilitate the activation of antigen-presenting cells and anti-tumour T cell responses. In other words, the innate immune sensing activity of STING is still considered to be central for its antitumour activity. However, whether and how STING exerts cell-intrinsic antitumour activity independent of its innate immune function remain unclear.

Increased aerobic glycolysis, or the Warburg effect, is another hallmark of cancer[17]. Cancer cells fuel the rapid metabolic demands with aerobic glycolysis to promote malignant cell proliferation[18]. Moreover, tumour aerobic glycolysis creates a hostile tumour microenvironment that leads to impaired antitumour immunity[19]. The depletion of local nutrients suppresses the proliferation and activation of antitumour T cells[19], while the accumulation of waste products (for example, lactate) reinforces the immunosuppressive environment[20,21]. However, whether and how tumour cell-intrinsic STING shapes aerobic glycolysis to regulate antitumour immunity are poorly understood.

In this article, we show that STING suppresses aerobic glycolysis independent of its innate immune function. STING targets HK2, a rate-limiting enzyme in glycolysis, to restrict aerobic glycolysis and promote antitumour immunity. Lactate production in human colorectal carcinomas is negatively correlated with STING expression and antitumour immunity. A naturally occurring STING(P2S) mutant loses the ability to target HK2 and restrict glycolysis. Together, these findings uncover a cell-intrinsic role of STING in the regulation of cellular metabolism and establish a critical link between the glycolysis-modulating and tumour suppressor activity of STING.

Results

STING suppresses aerobic glycolysis

While studying the function of STING, we constantly noticed that the culture medium of STING-deficient L929 cells turned yellow much quicker than that of wild-type (WT) cells (Extended Data Fig. 1a,b). These observations led us to speculate that STING may modulate aerobic glyco lysis. Depletion of STING abolished herring testis (HT)-DNA-induced expression of *Isg56* and *Cxcl10* as expected (Fig. 1a and Extended Data Fig. 1c). Notably, *Sting1*$^{-/-}$ L929 cells secreted much more lactate compared with WT cells (Fig. 1b). Both HT-DNA stimulation and HSV-1 infection led to STING degradation[22] (Extended Data Fig. 1d,e) and enhanced lactate production (Fig. 1c,d). Notably, STING-deficient L929 cells produced more lactate compared with WT cells, and HT-DNA stimulation and HSV-1 infection could not further enhance lactate generation (Fig. 1c,d).

To corroborate these findings, we blocked STING degradation with chloroquine or bafilomycin A1 (Extended Data Fig. 1f,g). Consistent with previous studies[23,24], bafilomycin A1 and chloroquine treatment augmented HT-DNA-induced innate immune signalling (Extended Data Fig. 1h). The secretion of lactate was significantly reduced by chloroquine or bafilomycin A1 treatment (Extended Data Fig. 1i,j). Moreover, STING retained at the ER by brefeldin A (BFA) treatment[25] inhibited lactate production (Extended Data Fig. 1k,l). TSG101 has been reported to be required for the lysosomal encapsulation and degradation of STING[26]. We confirmed that knockdown of the expression of *Tsg101* led to enhanced HT-DNA-induced innate immune signalling (Extended Data Fig. 2a,b). The stabilization of STING by *Tsg101* depletion suppressed lactate production (Extended Data Fig. 2c). Stimulated emission depletion (STED) super-resolution microscopy showed that STING localized to a reticular network without stimulation, and DMXAA (a STING agonist) treatment led to STING degradation. Consistent with previous reports, the depletion of *Atp6v1b2* (Extended Data Fig. 2d), a component of v-ATPase, and *Tsg101* impaired STING degradation; STING vesicles were encapsulated into lysosomal lumen in *Atp6v1b2*-depleted cells, whereas mRuby3–STING lingered and was peripherally associated with the lysosomal membrane in *Tsg101*-depleted cells[26] (Extended Data Fig. 2e). In BFA-treated cells, STING still localized to the ER after DMXAA stimulation (Extended Data Fig. 2f). We observed a fraction of STING vesicles localized in close vicinity to the lysosomal membranes but not in the lysosomal lumen after chloroquine and bafilomycin A1 treatment (Extended Data Fig. 2f), suggesting that treatment with bafilomycin A1 or chloroquine disrupts lysosome homeostasis, resulting in the accumulation of STING vesicles in the

cytosol[23]. We next stimulated the human monocyte cell line THP-1 with HSV-1 (ref. 27) and confirmed that STING degradation after HSV-1 infection coincided with higher production of lactate (Fig. 1e and Extended Data Fig. 2g).

To further validate these results, we performed rescue experiments (Fig. 1f) and found that STING reconstitution suppressed lactate production (Fig. 1g). Consistently, HT-DNA stimulation or HSV-1 infection led to the degradation of reconstituted STING (Extended Data Fig. 2h,i) and enhanced lactate generation in cells re-expressing STING (Fig. 1h,i). These data collectively indicate that STING suppresses lactate production. Seahorse analysis revealed that the basal extracellular acidification rate (ECAR) was comparable between WT and STING-deficient cells. The ECAR of *Sting1*$^{-/-}$ L929 cells after addition of glucose and oligomycin was higher than that of WT cells (Fig. 1j), indicating that the glycolic capacity of STING-deficient L929 cells was upregulated. STING reconstitution in STING-deficient cells repressed ECAR, again validating that STING suppresses aerobic glycolysis (Fig. 1k).

Taken together, these data indicate that STING suppresses aerobic glycolysis and lactate production.

STING restricts glycolysis independent of its innate role

Next, we examined whether the cell-intrinsic glycolysis-restriction activity of STING relies on its innate immune function. To answer this question, we took advantage of two well-defined STING mutants (S366A and R238A)—the S366A mutation abrogates the recruitment of IRF3, whereas R238A mutation disrupts cGAMP binding[22,28]. Reconstitution of WT STING (Extended Data Fig. 3a), but not the S366A and R238A mutants, restored HT-DNA-induced innate immune signalling in *Sting1*$^{-/-}$ L929 cells (Fig. 2a,d and Extended Data Fig. 3b). Notably, re-expression of the S366A and R238A mutants suppressed lactate production as efficiently as WT STING (Fig. 2b,e), suggesting that the innate immune function of STING is dispensable for its glycolysis restriction activity. HT-DNA stimulation or HSV-1 infection led to the degradation of STING(S366A) (Extended Data Fig. 3c) and enhanced the production of lactate (Fig. 2c). As the R238A mutation abrogates cGAMP binding and STING degradation (Extended Data Fig. 3d), HT-DNA stimulation or HSV-1 infection did not promote lactate production in STING(R238A)-reconstituted cells (Fig. 2f). These data indicate that the innate immune function of STING is dispensable for suppressing glycolysis.

We performed three sets of experiments to corroborate the conclusion. First, HT-DNA stimulation or HSV-1 infection induced the degradation of STING in cGAS-reconstituted cells but not in *Cgas*-knockout (KO) cells (Fig. 2g and Extended Data Fig. 3e–g). Although cGAS expression did not affect the lactate level, degradation of STING induced by HT-DNA or HSV-1 led to a higher production of lactate (Fig. 2h,i). Second, STING ablation promoted lactate production in IRF3-deficient cells (Extended Data Fig. 3h). Third, STING deficiency in *Ifnar1*$^{-/-}$ cells with defective type I IFN signalling led to an increased lactate level (Extended Data Fig. 3i–k). These data indicate that STING suppresses aerobic glycolysis independent of its innate immune function.

STING suppresses aerobic glycolysis by targeting HK2

To gain systemic insights into the metabolic perturbation imposed by STING, we depleted *Sting1* in L929 cells and performed metabolomics analysis. Consistent with previous reports[29], ablation of STING impaired the basal expression of a battery of IFN-stimulated genes and cytokines (Extended Data Fig. 4a). Unsupervised clustering showed that *Sting1* depletion greatly changed the cellular metabolic state (Extended Data Fig. 4b), and led to significant enrichment of glycolysis among other metabolic pathways (Fig. 3a). The enrichment of amino acid metabolism and glutathione metabolism pathways is consistent with the increasing demands for amino acids and heightened antioxidant capacity in cancer cells[30,31]. Specifically, *Sting1* depletion resulted in a higher amount of intracellular glycolytic metabolites, including fructose-6-phosphate, pyruvate, fructose-1,6-biphosphate, glyceral-3-phosphate (G3P), dihydroxyacetone phosphate and lactate (Fig. 3b and Extended Data Fig. 4c). We next fed WT and *Sting1*-KO L929 cells with isotope-labelled [U-^{13}C]glucose and monitor carbon fluxes. STING deficiency resulted in heightened labelling of the glycolytic intermediates (Fig. 3c and Extended Data Fig. 4d). These results corroborate that STING suppresses glycolysis.

To examine how STING inhibits glycolysis, we performed affinity purification coupled with proteomics analysis to identify the interacting partners of STING (Supplementary Table 1). Among the associated proteins, SURF4 has been reported to interact with STING and facilitate COPA-mediated retrieval of STING at the Golgi back to the ER[32,33]. HK2, which catalyses the rate-limiting step of the phosphorylation of glucose to generate glucose 6-phosphate during glycolysis, was also identified as a STING-binding protein (Fig. 3d). HK1 and HK2 are two major HKs, and *Hk2* depletion greatly reduced lactate production and cellular hexokinase (HK) activity, whereas *Hk1* depletion contributed slightly to these cellular activities[34] (Extended Data Fig. 4e,f). We therefore focused on HK2 in our study. We next confirmed that HK2 and STING formed a complex in cells (Fig. 3e and Extended Data Fig. 4g,h). Moreover, knockdown of *Tsg101* and treatment with BFA, chloroquine or bafilomycin A1 impaired HT-DNA-induced STING degradation, and STING could still interact with HK2 (Extended Data Fig. 5a–c). Purified STING associated with GST–HK2 but not GST, indicating that STING directly binds to HK2 (Fig. 3f). Using a proximity ligation assay (PLA), we further confirmed that endogenous STING and HK2 closely associated with each other (Fig. 3g). STED super-resolution microscopy revealed that HK2 spots were adjacent to, and partially co-localized with, ER-localized STING (Extended Data Fig. 5d,e). Domain-mapping experiments showed that the N-terminal transmembrane domain of STING (1–160) was required to interact with HK2 (Extended Data Fig. 5f). We next truncated HK2 into N- and C-terminal domains and found that both domains interacted with STING (Extended Data Fig. 5g). HK2 binds to the outer membrane of mitochondria through an N-terminal mitochondrial-binding motif[35,36], and an HK2 mutant (ΔN(1–16)) that loses mitochondrial localization could still interact with STING (Extended Data Fig. 5g). These data suggest that multiple domains of HK2 interact with STING independent of the mitochondrial localization of HK2.

Considering that HK2 is upregulated in many types of tumours[35] and STING interacts with HK2, we hypothesized that STING modulates HK2 activity. Indeed, HK activity was

significantly increased in STING-depleted cells (Fig. 3h). Re-expression of WT STING or the STING(S366A) or STING(R238A) mutants in STING-deficient cells effectively suppressed HK activity, indicating that STING inhibits HK2 activity independent of its innate immune function (Fig. 3i). As a control, restoration of cGAS in *Cgas*-KO cells did not affect HK activity (Extended Data Fig. 5h). Notably, the N-terminal transmembrane domain of STING was required to inhibit HK2 activity when reconstituted in STING-deficient cells (Extended Data Fig. 5i), consistent with our domain-mapping results. Moreover, HT-DNA stimulation or HSV-1 infection resulted in significantly elevated HK2 activity, whereas these treatments could not further upregulate HK2 activity in *Sting1*-depleted cells (Fig. 3j,k). We next purified HK2 and STING and found that purified STING inhibited HK2 activity in a dose-dependent manner (Extended Data Fig. 5j), suggesting that STING could directly suppress HK2 activity, possibly through a steric hindrance manner.

Taken together, these data indicate that STING interacts with HK2 and suppresses HK2 activity to restrict aerobic glycolysis.

STING inhibits HK2 mitochondrial localization and activity

The mitochondrial localization of HK2 is required for its activation[35]. We hypothesized that STING, localized at ER, may restrain HK2 and promote HK2 release from mitochondria. To test this hypothesis, we fractionated mitochondria and cytosol and found that depletion of STING indeed led to increased mitochondrial distribution of HK2 and decreased HK2 in the cytosol (Fig. 4a). To more directly evaluate the localization of HK2, we performed immunofluorescence staining and found that around 28% of HK2 was associated with the mitochondria in control cells; by contrast, around 63% of HK2 showed mitochondrial localization in STING-deficient cells (Fig. 4b and Extended Data Fig. 6a). These results suggest that STING impairs HK2 mitochondrial localization. Notably, a portion of HK2 was translocated to the Golgi and co-localized with STING after DMXAA stimulation (Extended Data Fig. 6b,c). Restoration of WT STING, STING(S366A) or STING(R238A) disrupted the mitochondrial localization of HK2 and enhanced HK2 cytosolic level, indicating that the innate immune function of STING is not required for repressing HK2 mitochondrial localization (Fig. 4c). HK2 associates with the mitochondrial outer membrane through its interaction with voltage-dependent anion channel 1 (VDAC1)[37]. Consistently, we observed that HK2 efficiently co-immunoprecipitated with VDAC1. Notably, the expression of STING nearly abolished the interaction between HK2 and VDAC1, suggesting that STING disrupts HK2–VDAC1 association to impair HK2 mitochondrial localization and activity (Fig. 4d). These results prompted us to further narrow down how STING restrains HK2. The deletion of N-terminal 14 amino acids abrogated the association between STING(1–160) and HK2 (Extended Data Fig. 6d). Further mutagenesis studies indicated that a proline to alanine mutation of the second amino acid (P2A) of STING disrupted its interaction with HK2 (Fig. 4e and Extended Data Fig. 6e). Multiple mutants showed a significant shift compared with WT STING, probably due to altered surfactant binding[38]. Consistently, the ΔN(1–14) and P2A mutants did not suppress HK2 activity when reintroduced into STING-deficient cells (Fig. 4f). As controls, WT STING and the P8A and I10A/P11A mutants effectively repressed HK2 activity (Fig. 4f). Moreover, reconstitution of WT STING, STING(P8A) or STING(I10A/P11A) in STING-deficient cells impaired HK2 mitochondrial

localization, whereas re-expression of STING(P2A) or STING(ΔN(1–14)) did not dissociate HK2 from the mitochondrial compartment to the cytosolic fraction (Fig. 4g). These data indicate that P2 of STING is required to associate with HK2 and block HK2 mitochondrial localization.

Next, we characterized the innate immune regulatory activities of these mutants. The STING(ΔN(1–14)) mutant did not activate an IFNβ reporter when co-expressed with cGAS[39] (Extended Data Fig. 6f). By contrast, the STING(P2A) mutant potently activated the IFNβ reporter, suggesting that the STING(P2A) mutant largely maintains the ability to initiate innate immune responses (Extended Data Fig. 6f).

Taken together, these data indicate that STING inhibits HK2 mitochondrial localization to block its HK activity.

STING targets HK2 to promote antitumour immunity in vivo

To determine whether STING restricts aerobic glycolysis in vivo, we turned to two widely used MC38 and CT26 colorectal carcinoma syngeneic mouse tumour models. First, we evaluated STING expression in these cell lines and found that MC38 cells expressed a low level of STING, whereas STING expression in CT26 cells was comparable to STING expression in L929 cells (Extended Data Fig. 7a). We therefore decided to introduce STING into MC38 cells and KO *Sting1* in CT26 cells to evaluate the role of STING in aerobic glycolysis and antitumour immunity. Stable expression of STING in MC38 cells markedly downregulated lactate production in vitro (Fig. 5a). STING introduction significantly slowed tumour growth in the MC38 tumour model (Fig. 5b,c) and downregulated lactate production in the tumours (Fig. 5d). Immunohistochemistry (IHC) staining of the mouse tumour tissues indicates that STING expression inhibited tumour cell proliferation and promoted apoptosis (Extended Data Fig. 7b). Moreover, STING expression in MC38 cells significantly increased lymphocyte infiltration (Extended Data Fig. 7c). Specifically, the percentage of tumour-infiltrating $CD8^+$ T cells, but not $CD4^+$ T cells, was enhanced in STING-expressing tumours (Fig. 5e and Extended Data Fig. 7d). Furthermore, around 5% of tumour-infiltrating $CD8^+$ T cells were PD1 and TIM3 double positive, denoting a severely exhausted T cell population, in STING-expressing MC38 tumours compared with about 16% of those in the control groups (Fig. 5e). STING expression also slightly reduced the percentage of severely exhausted $CD4^+$ T cells (Extended Data Fig. 7d). We also evaluated the percentage of $CD8^+$ and $CD4^+$ T cells in the spleens of the tumour-bearing mice and the exhaustion status. With the exception that the $CD8^+$ T cell percentage in the spleens showed a small but significant increase in STING-expressing MC38 tumour groups, the other parameters were comparable between the two groups (Extended Data Fig. 7e,f). Our results suggest that the elevated antitumour immunity by STING has a critical role in tumour suppression. To test this hypothesis, we performed MC38 tumour formation in NSG mice, which are severely immunodeficient and unable to mount antitumour immune responses. STING expression did not suppress tumour growth (Fig. 5f,g), although lactate production was decreased in STING-expressing tumours (Fig. 5h). IHC staining indicates that STING expression did not suppress tumour cell proliferation and promote apoptosis in NSG mice (Extended Data Fig.

7g). These data indicate that the immunomodulatory function of STING is central to its antitumour activity.

Depletion of *Sting1* in CT26 cells enhanced the production of lactate by around 20% (Fig. 5i,j). STING deficiency led to increased tumour burden and enhanced lactate in the tumour extracts (Fig. 5k,l). Moreover, STING deficiency promoted tumour cell proliferation and reduced apoptosis (Extended Data Fig. 8a). The intratumoural abundance of $CD8^+$ T cells was decreased, whereas the severely exhausted $CD8^+$ T cell populations were increased in STING-deficient tumours compared with those in the control groups (Fig. 5m), indicating that STING deficiency dampens antitumour immunity. By contrast, the intratumoural abundance of $CD4^+$ T cells and the exhaustion status were largely undisturbed (Extended Data Fig. 8b). The distribution and exhaustion status of $CD8^+$ and $CD4^+$ T cells in the spleens of the CT26 tumour-bearing mice were comparable (Extended Data Fig. 8c). By contrast, STING deficiency could not promote tumour growth in NSG mice despite the elevated lactate production (Extended Data Fig. 8d–g). These data indicate that STING restricts aerobic glycolysis and enhances antitumour immunity in vivo.

We next sought to establish a causal relationship between HK2 restriction by STING and the intrinsic tumour suppressor activity of STING in vivo. To test that, we turned to the two STING mutants (ΔN(1–14) and P2A) that could not bind to and inhibit HK2. WT STING but not the ΔN(1–14) and P2A mutants delayed tumour growth in the MC38 tumour model (Fig. 5n–p). Consistently, the ΔN(1–14) and P2A STING mutants lost the ability to suppress lactate production in MC38 tumours (Fig. 5q). In contrast to WT STING, both the ΔN(1–14) and P2A STING mutations did not increase the infiltration of lymphocytes and $CD8^+$ T cells in tumours (Fig. 5r). IHC staining further confirmed that the expression of STING(ΔN(1–14)) and STING(P2A) did not suppress tumour cell proliferation and promoted apoptosis as WT STING did (Extended Data Fig. 8h).

Together, these data indicate that STING targets HK2 to suppress aerobic glycolysis to promote antitumour immunity.

STING restricts aerobic glycolysis in established tumours

Our data indicate that STING suppresses aerobic glycolysis to modulate antitumour immunity. However, whether STING could still restrict glycolysis to promote antitumour immune responses in established tumours remains unclear. To address this question, we generated an MC38 stable cell line that enables doxycycline-inducible STING expression (Fig. 6a). We started to induce STING expression 8 days after implantation, when the tumour neovasculature had established. The induction of STING significantly inhibited tumour growth and reduced lactate production (Fig. 6b,c and Extended Data Fig. 9a). Furthermore, STING inducible expression promoted the infiltration of lymphocytes and $CD8^+$ T cells and reduced the populations of severely exhausted $CD8^+$ T cells (Fig. 6d,e and Extended Data Fig. 9b). By contrast, the infiltration of $CD4^+$ T cells and their exhaustion status were not significantly changed (Extended Data Fig. 9c,l). Notably, most tumour-infiltrating $CD8^+$ T cells expressed activation markers, with or without STING induction (Extended Data Fig. 9d,e,k). By contrast, the inducible expression of the STING(ΔN(1–14)) and STING(P2A) mutants (Fig. 6f) did not suppress tumour growth, reduce lactate

production or promote antitumour immunity (Fig. 6g–i and Extended Data Fig. 9f–i). To corroborate these results, we generated a CT26 stable cell line that enables doxycycline-inducible *Sting1* knockdown (Fig. 6j). Inducible knockdown of *Sting1* leads to enhanced tumour growth (Fig. 6k) and increased aerobic glycolysis, as demonstrated by enhanced glycolytic intermediates with in vivo isotope labelling (Fig. 6l). We wondered whether STING affects lactate production in mice. Notably, the lactate levels in the lung and serum were comparable between $Sting1^{+/+}$ and $Sting1^{-/-}$ mice, whereas the lactate levels in spleen, brain, skeletal muscle and heart of $Sting1^{-/-}$ mice were significantly increased compared with those of $Sting1^{+/+}$ mice (Extended Data Fig. 9j). These results indicate that STING deficiency enhances lactate levels in some organs in mice. These data collectively indicate that STING restricts aerobic glycolysis to promote antitumour immunity in established tumours.

HK2 is required for the tumour suppressor activity of STING

Our data demonstrate that STING targets HK2 to restrict aerobic glycolysis and inhibit tumorigenesis. We reason that *Hk2* depletion would abolish the cell-intrinsic tumour suppressor activity of STING. We performed two sets of experiments to test this hypothesis. First, we depleted *Hk2* and found that HK2 deficiency greatly diminished lactate secretion as expected (Fig. 7a,b). Notably, depletion of *Sting1* could not enhance lactate production in HK2-deficient cells as it did in control cells, suggesting that STING restricts glycolysis dependent on HK2 (Fig. 7c,d). We next found that depletion of *Sting1* resulted in enhanced tumour burden and increased lactate in the CT26 tumours, whereas depletion of *Hk2* delayed tumour growth and greatly downregulated lactate in the tumours (Fig. 7e–h), consistent with previous reports[34,40]. HK2 deficiency abrogated the glycolysis- and tumour-promoting activity of *Sting1* depletion in vivo (Fig. 7e–h). Moreover, STING deficiency reduced intratumoural abundance of $CD8^+$ T cells, but the immunomodulatory effect of STING disappeared when we depleted *Hk2* (Fig. 7i). The distribution of intratumoural $CD4^+$ T cells was not significantly changed in these groups (Fig. 7j). These data indicate that HK2 is required for the cell-intrinsic glycolysis restriction and tumour suppressor activity of STING.

STING regulates aerobic glycolysis in human CRC

To corroborate our findings with clinical relevance, we analysed a cohort of human colorectal adenocarcinoma (CRC) samples. IHC analysis indicated that representative CRC samples with high STING expression showed higher infiltration of T cells and $CD8^+$ T cells compared with those with low STING expression (Fig. 8a and Extended Data Fig. 10a). STING expression also correlated with enhanced T cell activation. Next, we found a significant negative correlation between the expression of STING and lactate. Furthermore, STING expression strongly correlated with $CD8^+$ T cell infiltration (*CD8A* and *CD8B*) and activation (*CD69*, *PRF1* and *IFNG*), whereas lactate negatively correlated with $CD8^+$ T cell infiltration and activation (Fig. 8b and Extended Data Fig. 10b,c). Previous studies indicate that carbonic anhydrase 9 (CA9) is upregulated in tumours with high lactate production and facilitates lactate efflux[41,42]. However, we did not find a significant correlation between the expression of CA9 and STING, or between CA9 and lactate in our patient cohort (Extended Data Fig. 10d). To expand our findings, we screened multiple human CRC cell

lines and found that HCT116 cells have a relatively high expression of STING, whereas the expression of STING in LoVo and RKO cells was almost undetectable (Extended Data Fig. 10e). We performed *STING1* KO or transduction to show that STING restricts lactate secretion in human CRC cells (Extended Data Fig. 10f). These results are consistent with a role for STING in the restriction of aerobic glycolysis and promotion of antitumour responses.

A STING(P2S) SNV does not restrict glycolysis

STING1 is highly heterogeneous in the human population[43,44]. Notably, rs1223377482 is a non-synonymous single-nucleotide variant (SNV) in *TMEM173* causing a Pro to Ser change at position 2 of STING. As a rare SNV, rs1223377482 was reported in both the Trans-Omics for Precision Medicine program (TOPMed) and the Genome Aggregation Database (GnomAD), with frequencies of 1/140,172 (GnomAD) and 1/264,690 (TOPMed). We predict that the rs1223377482 variant of STING might affect its glycolysis-modulating activity. Indeed, the P2S mutant of STING could not associate with HK2 and did not inhibit HK activity when reconstituted in STING-deficient cells (Fig. 8c–f). Moreover, the restoration of STING(P2S) in STING-deficient cells did not relocate HK2 from the mitochondria to the cytosol as WT STING did (Fig. 8g).

These data indicate that the naturally occurring STING(P2S) mutant loses the ability to target HK2 and restrict glycolysis.

Discussion

Previous studies revealed that STING expression is frequently silenced in a variety of human malignancies, including melanoma, colorectal, lung cancer and Merkel cell carcinoma, suggesting that STING functions as an intrinsic tumour suppressor[13–16]. In light of the intrinsic tumour suppressor activity of STING and its frequent epigenetic silencing in cancer cells, efforts have been taken to derepress STING to improve cancer therapy[14,45]. Moreover, STING agonists have achieved promising results in reviving antitumour immunity[46,47]. Oncolytic viruses exploit STING deficiency and have been shown to achieve better responses in STING-repressed tumours[13]. These STING-centred therapeutics are excellent strategies and would be valuable for the development of combination therapies with current cancer immunotherapies.

Compared with the extensive studies on STING in antiviral and antitumour immunity, our understanding of STING in the regulation of cellular metabolism is rudimentary. *Drosophila* STING contributes to lipid synthesis, and STING-depletion mutants are sensitive to starvation[48]. Notably, some cancer cells exhibit simultaneous silencing of cGAS and STING, suggesting that these proteins possess functions independent of their innate immune activities[15,45]. Indeed, cGAS inhibits DNA-damage repair and suppresses genome instability independent of STING[49–51]. Our study establishes that cancer-cell-intrinsic STING modulates aerobic glycolysis to boost antitumour immunity independent of its innate immune function. These findings offer valuable insights into potential therapeutic strategies for targeting cancer metabolism in tumours with repressed STING expression. For example, monocarboxylate transporter 4 (MCT4) has been established as a high-affinity transporter

that mediates lactate efflux[52]. On the basis of our studies, we propose that targeting MCT4 can be a potential strategy to treat tumours with silenced STING.

Previous studies have established that the ER–Golgi trafficking of STING is required for innate immune activation[25,53], and STING subsequently translocates to the lysosome for degradation. Recent studies have started to reveal how STING reaches the lysosome. Clathrin-coated vesicles and the ESCRT complex are required for the delivery and encapsulation of STING into the lysosome[26,54]. Notably, a fraction of STING vesicles localize in close proximity to lysosomal membranes but not in lysosomal lumen with chloroquine and bafilomycin A1 treatment, suggesting that these treatments disrupt lysosome homeostasis, resulting in the accumulation of STING vesicles in the cytosol.

In summary, we report here that STING restricts aerobic glycolysis by targeting HK2 to promote antitumour immunity. The aerobic glycolysis activity of human colorectal carcinoma samples is negatively correlated with STING and antitumour immunity. A naturally occurring STING variant that cannot associate with HK2 loses the ability to restrict glycolysis. Our studies not only establish an important link between the intrinsic tumour suppressor activity of STING and cellular metabolism, but also have critical implications for the development of therapeutic modalities that target STING or lead to STING degradation.

Online content

Any methods, additional references, Nature Portfolio reporting summaries, source data, extended data, supplementary information, acknowledgements, peer review information; details of author contributions and competing interests; and statements of data and code availability are available at https://doi.org/10.1038/s41556-023-01185-x.

Methods

Ethical approval

A statement of informed consent was obtained from the patients with CRC. No compensation was provided. The study protocol was approved by the Medical Ethics Committee of Zhongnan Hospital, Wuhan University and the Medical Ethics Committee of Medical Research Institute, Wuhan University. Animal studies were approved by the Animal Care and Ethics Committee of Medical Research Institute, Wuhan University.

CRC samples from a cohort of 84 individuals (the scientists were blinded to the patient information, including sex, gender and age, to protect confidentiality) were collected at the Department of Colorectal and Anal Surgery, Zhongnan Hospital of Wuhan University (Wuhan, China) from May 2020 to November 2020. Each tumour sample was rinsed with PBS and split into three parts for IHC, quantitative PCR with reverse transcription (RT–qPCR) and lactate measurement.

Mice

C57BL/6J mice and BALB/c mice were purchased from the Hu'nan SJA Laboratory. NSG mice (NOD-*Prkdc*^{scid}*Il2rg*^{em1}*/Smoc*) were purchased from Shanghai Model Organisms Center. The *Ifnar1*$^{-/-}$ mice (B6.129S2-*Ifnar1*^{tm1Agt}/Mmjax) were provided by X. Zhou

(Wuhan Institute of Virology). The *Sting1*$^{-/-}$ mice provided by H.-B. Shu and B. Wu were on the C57BL/6J background (Wuhan University). Mice of either sex on a normal chow diet (13% fat, 57% carbohydrate and 30% protein; Beijing Keao Xieli Feed, 23033313) were kept in a specific-pathogen-free facility (12 h–12 h light–dark cycle, humidity of 40–50%, 22 ± 2 °C) at the Medical Research Institute, Wuhan University. Mice aged 6–8 weeks were used in all of the experiments.

MC38 (1×10^6) or CT26 (5×10^6) cells were resuspended in PBS and mixed with Matrigel (356237, Corning) at a 2:1 volume ratio, and 100 μl of the suspension was implanted subcutaneously into the right flank of the mice. The tumour size was measured using digital callipers every other day. The tumour volume was calculated using the modified ellipsoid formula $V = (L \times l^2)/2$, where L and l are the widest and the smallest diameter, respectively. The maximal tumour size permitted by the ethics committee is 1.8 cm^3 for a single tumour. We confirm that the maximal tumour size was not exceeded in any of the experiments.

For Dox-inducible STING expression in vivo, MC38 (5×10^4) cells stably transduced with pLVX-TetOne-Puro, pLVX-TetOne-Flag-STING or the mutants were implanted subcutaneously into C57BL/6J mice. For Dox-inducible shRNA-mediated knockdown of *Sting1* in vivo, CT26 (1×10^6) cells were stably transduced with Tet-pLKO-puro-sh-control or Tet-pLKO-puro-sh-STING. Dox-containing chow diet (200 mg kg^{-1}) (Custom diet, Jiangsu Xietong Pharmaceutical Bio-engineering) was given when the tumours were established on day 8 after implantation. At day 16 after implantation, the mice bearing CT26 tumours were maintained anaesthesia by isoflurane inhalation for 150 min. [U-^{13}C]glucose (CLM-1396–1, Cambridge Isotope Laboratories) (20 mg kg^{-1} min^{-1}) was administrated through tail vein injection controlled by an automatic injector (injection rate, 150 μl h^{-1}). At the end of the labelling, the mice were immediately euthanized and the tumours were collected for metabolite extraction. The preparation of metabolic extracts and the analysis are described in the ‘Metabolomics and isotope tracing metabolomics’ section.

Cells and viruses

HEK293T (ATCC-CRL-3216), U2OS (ATCC-HTB-96), HeLa (ATCC-CCL-2), VERO (ATCC-CCL-81), HCT116, LoVo, RKO, L929, MC38 and CT26 cells were cultured in Dulbecco’s modified Eagle’s medium (DMEM, Sigma-Aldrich) with 10% fetal calf serum (FCS), supplemented with penicillin (100 U ml^{-1}) and streptomycin (100 mg ml^{-1}) (Hyclone). THP-1 cells (ATCC-TIB-202) were cultured in RPMI 1640 medium (Sigma-Aldrich) supplemented with 10% FCS and penicillin–streptomycin. L929 WT and *Cgas*$^{-/-}$ cells were provided by J. Chen (UT Southwestern Medical Center). MC38 and CT26 cells were provided by J. Zhang, W. Song and C. Cai (Wuhan University). *Sting1*$^{+/+}$ and *Sting1*$^{-/-}$ MLFs were provided by Q. Yang and H.-B. Shu (Wuhan University). HCT116, LoVo and RKO cells were provided by H. Liu (Wuhan University). Primary WT and *Ifnar1*$^{-/-}$ MLFs were generated and cultured as previously described[27]. The gender of the cell lines was not a consideration in this study. The cell lines were not authenticated.

HSV-1 and HSV-1-ΔICP0 (F strain) were propagated using VERO Cells[55].

Constructs and reagents

Expression plasmids for HA-tagged or Flag-tagged STING and its mutants, and Flag–HK2 and its mutants, were constructed using standard molecular biology techniques. Mammalian expression plasmids for HA-tagged STING (1–379, 1–160, 1–190, 151–379, 191–379, 221–379) were provided by H.-B. Shu[56]. sgRNA targeting *Sting1*, *Hk2*, *Hk1* and *Irf3* was constructed into Lenti-CRISPRv2 vector (52961, Addgene). shRNA targeting mouse *Sting1* was cloned into Tet-pLKO-puro vector (provided by H. Du (Wuhan University)). The sequences for sgRNA and shRNA used in this study are listed in Supplementary Table 2.

The reagents were purchased from the following companies: IFNβ (PeproTech), HT-DNA and chloroquine (Sigma-Aldrich), bafilomycin A1, BFA, 2DG, DMXAA and doxycycline (MedChemExpress).

Stable cell line generation

Lentiviruses were generated in HEK293T cells as previously described[57]. In brief, HEK293T cells were transfected with the lentiviral expression plasmids together with psPAX2 (12260, Addgene) and pVSV-G (8454, Addgene). At 48 h after transfection, lentiviruses were collected and used to infect the indicated cells in the presence of polybrene (4 μg ml^{-1}). The infected cells were selected with puromycin (2 μg ml^{-1} for MLF, MC38, CT26 and HCT116 or 4 μg ml^{-1} for L929 cells) or hygromycin (200 μg ml^{-1} for MC38 or 400 μg ml^{-1} for L929, MLF, LoVo and RKO cells) for 5 days.

Immunoprecipitation and immunoblotting

Immunoprecipitation was performed to assess protein–protein interactions[58]. In brief, HEK293T cells were transfected with the expression constructs. Cells were collected at 24 h after transfection and lysed with NP40 buffer (50 mM Tris-HCl, pH 7.4, 150 mM NaCl, 1% NP-40, 1 mM EDTA, 5% glycerol) supplemented with a protease inhibitor cocktail. Centrifuged cell lysates were incubated with 10 μl of anti-Flag-M2 affinity gel (Sigma-Aldrich) for immunoprecipitation of Flag-tagged proteins. For endogenous immunoprecipitation, THP-1 cell extracts were prepared and incubated with 0.5 μg of STING or HK2 antibody plus 10 μl of protein G-agarose (GE Healthcare) at 4 °C for 4 h. Agarose beads were washed three times with lysis buffer and boiled with 1× SDS sample buffer at 95 °C for 10 min. L929 cells were pretreated with BFA (10 μg ml^{-1}), chloroquine (20 μM) or bafilomycin A1 (400 nM) for 30 min and then stimulated with HT-DNA (1 μg ml^{-1}) for 12 h. For *Tsg101* depletion, L929 cells were transfected with control short interfering RNA (siRNA) or *Tsg101* siRNA for 60 h and then stimulated with HT-DNA (1 μg ml^{-1}) for 12 h. L929 whole-cell extracts were prepared, and anti-STING antibodies were used for immunoprecipitation. A list of the antibodies used in this study is provided in Supplementary Table 3.

Preparation of single-cell suspensions from mouse tumours

Tumours were cut into small pieces (around 2–4 mm in diameter) and transferred into a MACS gentle dissociator C tube (130–093-237, Miltenyi Biotech) with an enzyme mix containing 2.35 ml DMEM, 100 μl enzyme D, 50 μl of enzyme R and 12.5 μl enzyme A from a tumour dissociation kit (Miltenyi Biotec). The C tube was tightly closed and

installed onto the sleeve of the gentleMACS Octo Dissociator (Miltenyi Biotec), and then the dissociation of the tumour was performed. After completion of the dissociation program, the digested cell mixture was incubated at 37 °C for 30 min and filtered through 70 μm MACS SmartStrainers (130–098-465, Miltenyi Biotec) to collect single-cell suspensions.

Flow cytometry

Tumour single-cell suspensions were washed twice with 2% FBS/1× PBS staining buffer and treated with red blood cell lysis buffer (BL503B, Biosharp) for 3 min. Zombie Violet fixable viability dye (423114, Bio-Legend) was used to exclude dead cells. Cells were incubated with mouse CD16/32 antibodies to saturate Fcγ receptors for 10 min and then stained with antibodies against cell surface molecules for 30 min at 4 °C. Flow cytometry data were acquired on the BD LSRFortessa X-20 cell analyser (BD Biosciences) and analysed using FlowJo software. A list of the antibodies used for flow cytometry in this study is provided in Supplementary Table 3.

Metabolomics and isotope tracing metabolomics

Control or *Sting1*$^{-/-}$ L929 cells (2×10^6, four replicates per sample) were collected for metabolic profiling experiments. The cells were resuspended with prechilled 500 μl of suspension buffer containing 80% methanol and 0.1% formic acid. The samples were incubated on ice for 5 min, followed by centrifugation (15,000*g*) at 4 °C for 10 min. The supernatant was diluted to a final concentration containing 53% methanol. The samples were then transferred to a fresh Eppendorf tube and centrifuged (15,000*g*) at 4 °C for 20 min. The metabolite intensities were analysed by LC–MS/MS (Novogene). LC–MS/MS analyses were performed using an ExionLC AD system (SCIEX) coupled with a QTRAP 6500+ mass spectrometer (SCIEX).

For isotype tracing, control or *Sting1*$^{-/-}$ L929 cells (2×10^6) were washed three times with PBS and refreshed with DMEM without glucose (11966025, Gibco), supplemented with 4.5 g l^{-1} [U-$^{13}C_6$]D-glucose (CLM-1396–1, Cambridge Isotope Laboratories). After 1 h of labelling, metabolic extracts were isolated by cold methanol extraction as described for the metabolomics analysis. All of the samples were run in biological triplicate. Metabolites in the supernatant were dried at room temperature under a vacuum and resuspended in water for LC–MS analysis (Tsinghua metabolomics core, Tsinghua University). Incorporation of ^{13}C into metabolites extracted from cells was performed using a Dionex Ultimate 3000 UPLC system as previously described[59].

The metabolites were annotated using the KEGG database (http://www.genome.jp/kegg/), HMDB database (http://www.hmdb.ca/) and Lipidmaps database (http://www.lipidmaps.org/). Principal component analysis and partial least-squares discriminant analysis were performed using metaX[60]. Univariate *t*-tests were applied to calculate the statistical significance (*P* value). Volcano plots were used to filter metabolites of interest based on the $\log_2$-transformed fold change and $-\log_{10}$-transformed false-discovery rate of metabolites. For clustering heat maps, the data were normalized using *z*-scores of the intensity areas of differential metabolites and were plotted using heatmap package in R.

The functions of these metabolites and metabolic pathways were analysed using the KEGG database.

Measurement of ECAR

ECAR was measured using the Agilent seahorse XF glycolysis stress test kit (103020–100, Seahorse Biosciences). In brief, 6×10^4 cells were seeded into XFe96 Cell Culture Microplates (101085–004, Seahorse Bioscience) and cultured in a 37 °C incubator containing 5% CO_2 for 12 h. After washing with assay medium (102353–100, XF Base Medium Minimum DMEM), the cells were kept in a CO_2-free incubator at 37 °C for 1 h before the measurement. For the measurement of ECAR, three injections (glucose (10 mM), oligomycin (1 μM) and 2-DG (50 mM)) were performed at the indicated timepoints. ECAR values were normalized to the total amount of proteins. All of the experiments were conducted in triplicate. ECAR parameters were calculated using Seahorse XF-24 software according to the manufacturer's instructions. The basal glycolysis, glycolytic capacity and glycolytic reserve were analysed and visualized using Wave software (v.2.3.0, Seahorse Bioscience, Agilent Technologies).

Measurement of HK activity

Mitochondria were isolated using the mitochondrial extraction kit (SM0020, Solarbio) according to the manufacturer's manual. In brief, 5×10^7 L929 cells were collected and resuspended in 1 ml of lysis buffer, and transferred to a prechilled dounce homogenizer. After 40 grinds, the samples were centrifuged at 1,000*g* for 5 min at 4 °C. The supernatants were further centrifuged at 12,000*g* for 10 min at 4 °C. The mitochondrial pellets were washed with washing buffer twice, resuspended in store buffer. HK activity was measured using the Hexokinase Colorimetric Assay Kit (K789–100, Biovision) according to the manufacturer's instructions.

Measurement of lactate

Lactate levels were measured using the Lactate Colorimetric/Fluorometric Assay Kit (K6027–100, Biovision). Cells were seeded in 12-well plates at a density of 1×10^5 cells per well, and the culture medium was collected for lactate measurement according to the manufacturer's instructions.

Tumour tissues and organs of *Sting1*$^{+/+}$ or *Sting1*$^{-/-}$ mice were weighted and homogenized in ten volumes of DMEM using a mechanical homogenizer. The lysates were then centrifuged at 14,000*g* for 10 min at 4 °C, and the supernatants were applied to lactate detection.

Protein purification

GST–HK2 was expressed in *Escherichia coli* BL21-DE3 cells, and the induction was performed with 0.5 mM IPTG at 18 °C overnight. Bacterial pellets were collected and sonicated in lysis buffer (20 mM Tris-Cl, pH 8.0, 150 mM NaCl, 5% glycerol, 1% Triton X-100, 0.2 mM PMSF, 0.25 mg ml^{-1} lysozyme) on ice for 30 min. After centrifugation, the supernatant was collected and incubated with glutathione Sepharose 4B (17–0757-01, GE Healthcare) for 4 h at 4 °C. GST–HK2 bound to glutathione Sepharose beads was washed

extensively with washing buffer (20 mM Tris-Cl, pH 8.0, 150 mM NaCl, 5% glycerol) and eluted with GST elution buffer (20 mM reduced glutathione, 20 mM Tris-Cl, pH 8.0, 150 mM NaCl).

Flag–STING was purified by affinity purification from HEK293T cells as previously described[57]. In brief, HEK293T cells were transfected with Flag–STING. At after 24 h transfection, cells were collected and lysed in lysis buffer (50 mM Tris-HCl, pH 7.4, 150 mM NaCl, 1% NP-40, 1 mM EDTA, 5% glycerol) supplemented with a protease inhibitor cocktail. Centrifuged cell lysates were incubated with 40 μl of anti-Flag-M2 affinity gel (A2220, Sigma-Aldrich) at 4 °C for 4 h. Flag–STING was then eluted by incubating with Flag peptide (400 μg ml^{-1}, Bimake) for 4 h at 4 °C.

In vitro HK enzymatic activity

HK enzymatic activity in vitro was measured using purified GST–HK2 incubated with purified Flag–STING in the reaction buffer (20 mM Tris-Cl, pH 8.0, 150 mM NaCl, 2 mM $MgCl_2$, 1 mM DTT, 5% glycerol) in the presence of ATP (50 μM) (R0441, Thermo Fisher Scientific) for 1 h at 37 °C. The HK2 enzymatic activity was then measured using the Hexokinase Colorimetric Assay Kit (K789–100, Biovision).

GST pull-down assay

A total of 1 μg of GST–HK2 coupled to the glutathione beads was equilibrated with binding buffer (20 mM Tris-HCl, pH 8.0, 100 mM NaCl, 1% NP-40, 1 mM EDTA, 1 mM PMSF) and incubated with purified Flag–STING for 4 h at 4 °C. After incubation, the beads were centrifuged and washed with pull-down buffer (20 mM Tris, pH 8.0, 0.1% Triton X-100, 150 mM NaCl, 1 mM DTT). Bound proteins were eluted by boiling with 1× SDS loading buffer for 10 min and analysed using immunoblotting.

RNA extraction and RT–qPCR

Total RNA of cells or tumour tissues was extracted using TRIzol reagent (9109, Takara). Total RNA (1 μg) was used for reverse transcription with HiScript II Reverse Transcriptase (R201–01, Vazyme) according to the manufacturer's instructions. qPCR was performed with the SYBR Green qPCR Master Mix (B21203, Bimake) using the Bio-Rad CFX Connect Real-Time PCR Detection System.

The expression of the target genes was normalized to the house keeping genes (*RNA18S* or *ACTB* for human genes and *Actb* for mouse genes). The quantification was performed in biological triplicates, and error bars show the s.d. A list of the primers used for qPCR is provided in Supplementary Table 2.

RNA-seq analysis

Control or *Sting1*$^{-/-}$ L929 cells (2×10^6, three replicates per sample) were collected, and total RNA was isolated with TRIzol reagent according to the manufacturer's instructions.

Oligo(dT)-attached magnetic beads were used to purify mRNA. A sequencing library was constructed, and RNA sequencing was performed using the BGISEQ500 platform (BGI).

The sequencing data were filtered using SOAPnuke (v.1.5.2), and the clean reads in FASTQ format were mapped to the reference genome using HISAT2 (v.2.0.4). Bowtie2 (v.2.2.5) was used to align the clean reads to the reference coding gene set, then the gene expression level was calculated using RSEM (v.1.2.12). Differential expression analysis was performed using DESeq2 (v.1.4.5). The heat map was drawn using pheatmap (v.1.0.8) according to the gene expression data.

Luciferase reporter assay

Luciferase reporter assays were performed using a dual-specific luciferase assay system (E1910, Promega)[61]. HEK293T cells were transfected with a reporter plasmid mixture containing the plasmid expressing IFNβ firefly luciferase reporter, TK-*Renilla* luciferase reporter, cGAS and STING, or the indicated mutants. At 24 h after transfection, cells were collected and the cell lysates were used for the dual luciferase assay according to the manufacturer's instructions.

Immunofluorescence staining

For the detection of STING and the lysosome, *Sting1*$^{-/-}$ MLF cells stably expressing mRuby3–mSTING and LAMP1–eGFP were transfected with control siRNA, *Atp6v1b2* siRNA or *Tsg101* siRNA (20 nM) (RiboBio) for 60 h and then simulated with DMXAA (25 μg ml^{-1}) for 12 h. For the inhibitor treatment, *Sting1*$^{-/-}$ MLF cells stably expressing mRuby3–mSTING and LAMP1–eGFP were stimulated with DMXAA (25 μg ml^{-1}) and treated with BFA (10 μg ml^{-1}), chloroquine (20 μM) or bafilomycin A1 (400 nM) for 12 h.

For the detection of STING, HK2 and the Golgi, *Sting1*$^{-/-}$ MLF cells stably expressing eGFP–mSTING were stimulated with DMXAA (25 μg ml^{-1}) for 30 min.

For the detection of HK2 and the mitochondria, *Sting1*$^{+/+}$ and *Sting1*$^{-/-}$ MLF cells were labelled with MitoTracker (100 ng ml^{-1}) (M7512, Invitrogen) at 37 °C for 15 min. For the detection of STING, HK2 and the mitochondria, *Sting1*$^{-/-}$ MLF cells stably expressing eGFP–mSTING were labelled with MitoTracker (100 ng ml^{-1}) at 37 °C for 15 min and then stimulated with DMXAA (25 μg ml^{-1}) for 30 min.

For the detection of STING, HK2 and the ER, *Sting1*$^{-/-}$ MLF cells stably expressing eGFP–mSTING were processed for immunostaining.

Cells were fixed with 4% (v/v) paraformaldehyde for 10 min, followed by permeabilization with 0.1% (w/v) Triton X-100 for 5 min. After being blocked with 10% normal goat serum in PBS for 1 h at room temperature, the samples were incubated with primary antibodies at 4 °C overnight. After washing, cells were incubated with species-specific secondary antibodies for 1 h at room temperature. Finally, the slides were mounted with ProLong Gold mounting medium (Thermo Fisher Scientific). Images were acquired using the Abberior STEDYCON (Abberior Instruments) fluorescence microscope with a motorized inverted microscope IX83 (Olympus UPlanXAPO 100x).

All of the images were analysed using the STEDYCON gallery software (Abberior Instruments). The fluorescence-intensity profiles were generated using Microsoft Excel

2016. The Pearson's correlation coefficient between HK2, and mitochondria was calculated using Coloc2 in Image J (NIH).

A list of the primary antibodies and secondary antibodies used for immunofluorescence staining is provided in Supplementary Table 3.

PLA analysis

To detect in situ HK2–STING interaction, the PLA was conducted using the Duolink kit (DUO92101, Sigma-Aldrich) according to the manufacturer's instructions. HeLa cells were fixed with 4% paraformaldehyde for 10 min, permeabilized in 0.1% Triton X-100 for 5 min followed by blocking with 10% goat serum for 1 h. Cells were then incubated overnight with rabbit anti-STING polyclonal antibodies and mouse anti-HK2 monoclonal antibodies. After washing, cells were incubated with secondary antibodies conjugated to PLA probe at 37 °C for 1 h. Ligation and amplification were then performed, and the slides were mounted with ProLong Gold mounting medium. The images were acquired by confocal microscopy (LSM880, Zeiss).

Immunohistology

Formalin-fixed and paraffin-embedded tissues were sectioned continuously at a thickness of 4 μm. The sections were deparaffinized with xylene for 15 min three times and rehydrated in 100%, 85% and 70% ethanol for 5 min. The sections were then placed into antigen retrieval buffer with citric acid (pH 6.0) for antigen retrieval. Subsequently, the sections were placed into 3% hydrogen peroxide and incubated at room temperature for 25 min to block endogenous peroxidase activity. After being blocked with 3% BSA in PBS for 1 h at room temperature, the sections were stained with primary antibodies diluted in PBS containing 1% BSA and incubated at 4 °C overnight. The sections were then incubated with HRP-conjugated secondary antibodies at room temperature for 1 h. The diaminobenzidine chromogenic agent kit (G1211, Servicebio) was used for detection. Images were acquired using the Leica Aperio VERSA 8 multifunctional scanner. The percentage of Ki-67-positive or cleaved caspase-3-positive cells was quantified using Image J (NIH). A list of the antibodies used for IHC is provided in Supplementary Table 3.

Statistics and reproducibility

Data represent the mean of at least three independent experiments, and error bars denote the s.d. unless specified otherwise. Two-tailed Student's *t*-tests were performed for pairwise comparisons. The number of independent biological experiments and replicates (*n*) is indicated in the figure legends. Pearson's $\chi 2$ tests were used to analyse the correlation between tissue gene expression and lactate. GraphPad Prism 8 was used for statistical analysis.

No statistical methods were used to predetermine sample sizes, but our sample sizes are similar to those reported in previous publications[27]. No data were excluded from the analyses. The experiments were not randomized. Data collection and analysis were not performed blinded to the conditions of the experiments. Data distribution was assumed to be normal, but this was not formally tested.

Reporting summary

Further information on research design is available in the Nature Portfolio Reporting Summary linked to this article.

Extended Data

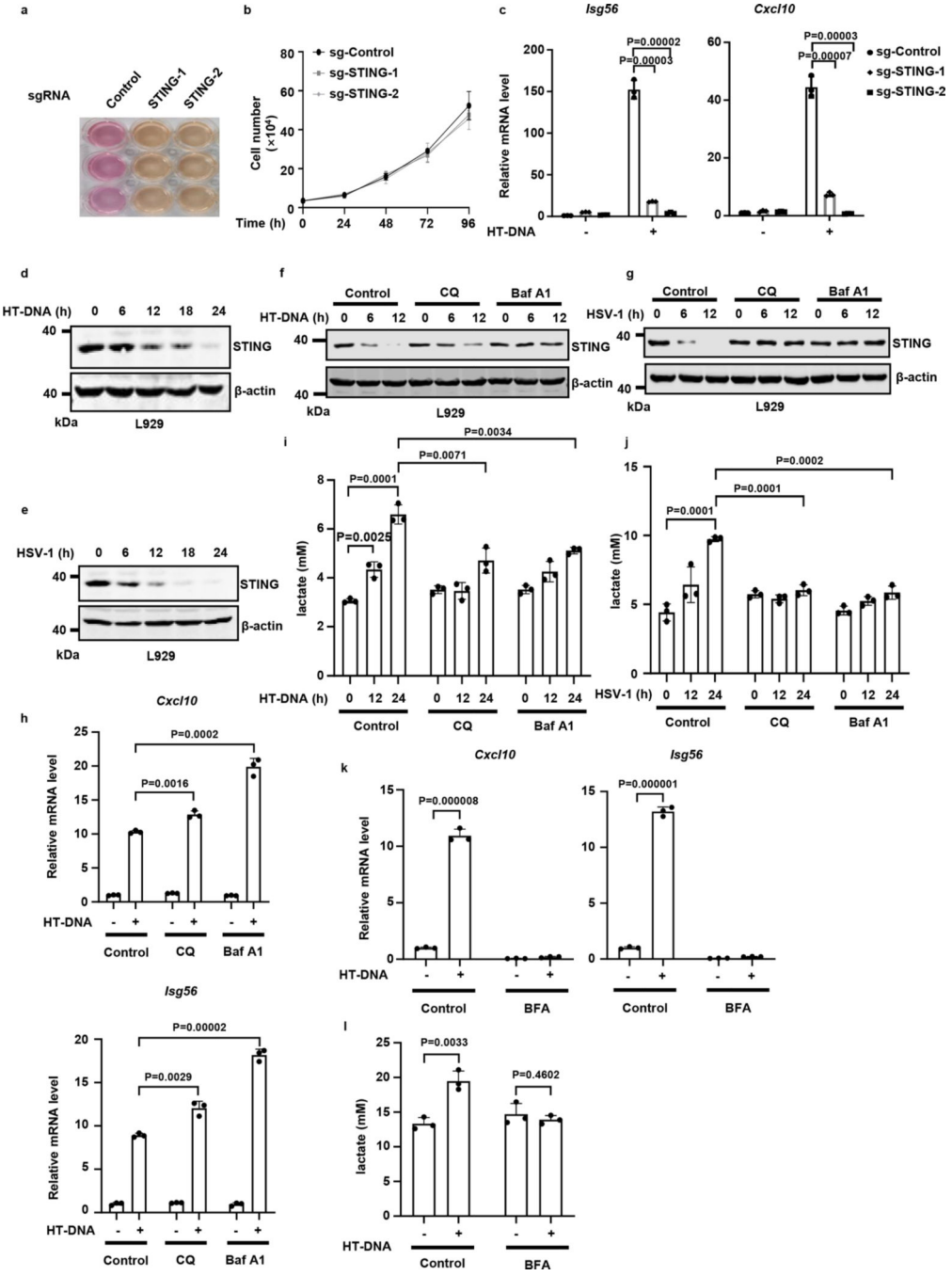

Extended Data Fig. 1 |. STING restricts aerobic glycolysis.

a, Image of the colour of the cell culture media. **b**, the number of control or *Sting1*$^{-/-}$ L929 cells was quantified at the indicated time points. **c**, qPCR analysis of *Isg56* or *Cxcl10* mRNA in control or *Sting1*$^{-/-}$ L929 cells transfected with or without HT-DNA. **d and e**, immunoblotting analysis of L929 cells transfected with HT-DNA or infected with HSV-1. **f**, L929 cells were pre-treated with chloroquine (20 μM) or bafilomycin A1 (400 nM) for 30 minutes and then transfected with HT-DNA (1 μg/ml), followed by immunoblotting. **g**, L929 cells were infected with HSV-1 (MOI = 1) and treated with chloroquine (20 μM) or bafilomycin A1 (400 nM). WCLs were analysed by immunoblotting. **h**, L929 cells were pre-treated with chloroquine (20 μM) or bafilomycin A1 (400 nM) for 30 minutes and then transfected with HT-DNA (1 μg/ml). The expression of *Cxcl10* and *Isg56* was quantified at 8 h post-transfection. **i**, L929 cells were pre-treated with chloroquine (20 μM) or bafilomycin A1 (400 nM) for 30 minutes and then transfected with HT-DNA (1 μg/ml), followed by lactate meaturement. **j**, L929 cells were infected with HSV-1 (MOI = 1) and treated with chloroquine (20 μM) or bafilomycin A1 (400 nM). Lactate was measured at the indicated time points. **k**, L929 cells were pre-treated with brefeldin A (10 μg/ml) for 30 minutes and then transfected with HT-DNA (1 μg/ml). The expression of *Cxcl10* and *Isg56* was quantified at 8 h post-transfection. **l**, L929 cells were transfected with HT-DNA (1 μg/ml) and treated with brefeldin A (10 μg/ml). lactate was measured at 24 h post-transfection. Data are presented as means ± s.d. of n = 3 independent biological replicates for **b**, **c**, **h-l**. P-value was calculated by two-tailed Student's t-test. Data are representative of three independent experiments. Uncropped gel images and numerical data are available in source data.

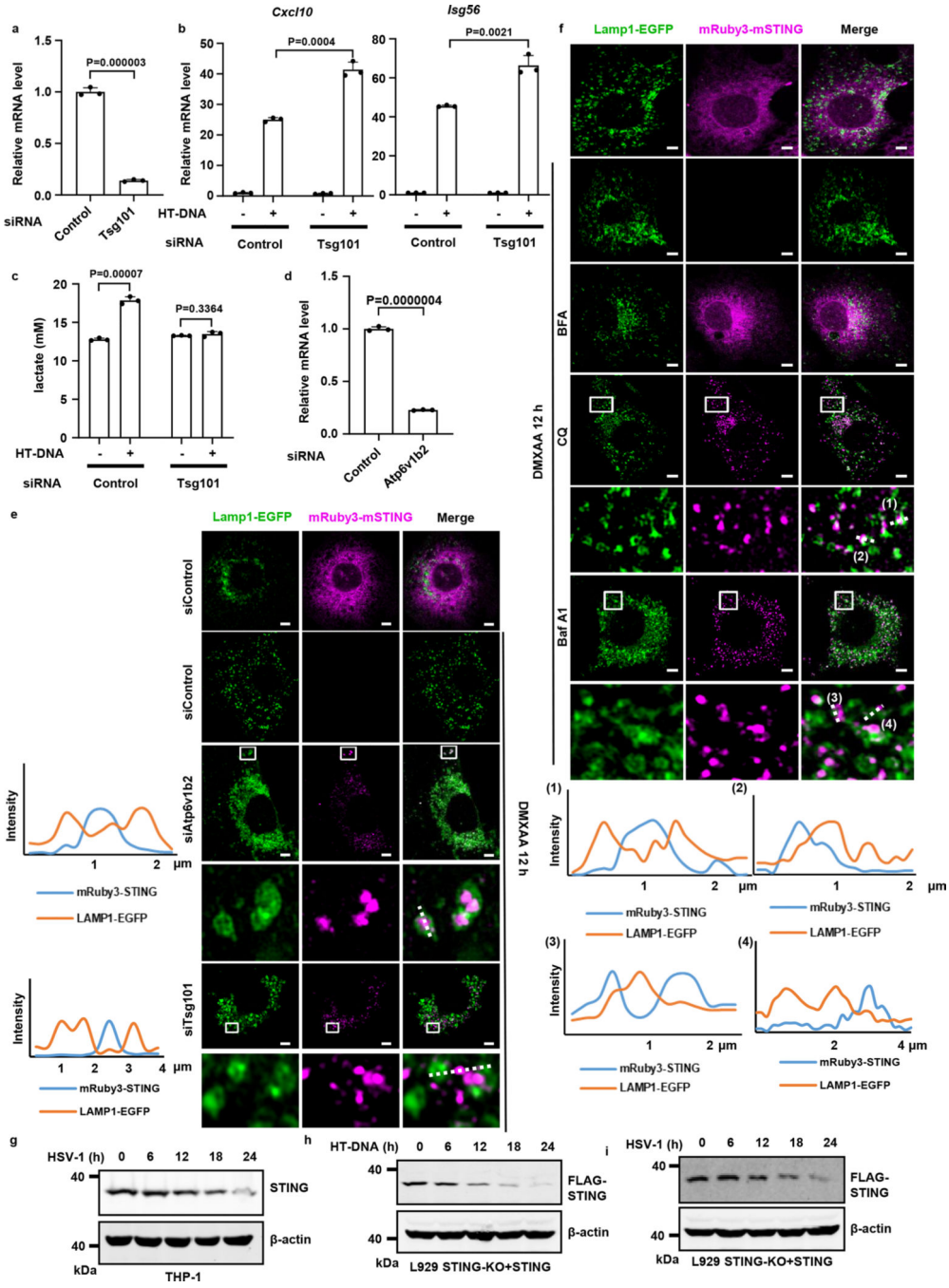

Extended Data Fig. 2 |. STING vesicles retained in the cytosol by Baf A1 or CQ restricts aerobic glycolysis.

a, L929 cells were transfected with control siRNA or *Tsg101* siRNA, and the expression of *Tsg101* was quantified at 72 h post-transfection. **b**, L929 cells from (**a**) were stimulated with HT-DNA (1 μg/ml) for 8 h. The expression of *Cxcl10* and *Isg56* was quantified by qPCR. **c**, L929 cells from (**a**) were stimulated with HT-DNA (1 μg/ml) for 24 h, followed by lactate measurement. **d**, L929 cells were transfected with Control siRNA or *Atp6v1b2* siRNA, and the expression of *Atp6v1b2* was quantified at 72 h post-transfection. **e**, *Sting1*$^{-/-}$ MLF cells

stably expressing mRuby3-mSTING and Lamp1-EGFP were treated with control siRNA, *Atp6v1b2* siRNA or *Tsg101* siRNA for 60 h, and then stimulated with DMXAA (25 μg/ml) for 12 h. Cells were fixed and imaged by STED super-resolution microscopy. Scale bars, 5 μm. The boxed areas in the top panels were magnified in the bottom, and the fluorescence intensity profiles along the white dotted lines were shown. **f**, *Sting1*$^{-/-}$ MLF cells stably expressing mRuby3-mSTING and Lamp1-EGFP were stimulated with DMXAA (25 μg/ml), and treated with brefeldin A (10 μg/ml), chloroquine (20 μM), or bafilomycin A1 (400 nM) for 12 h. Cells were fixed and imaged by STED super-resolution microscopy. Scale bars, 5 μm. The boxed areas in the top panels were magnified in the bottom, and the fluorescence intensity profiles along the white dotted lines were shown. **g**, immunoblotting analysis of THP-1 cells infected with HSV-1 (MOI = 1). **h** and **i**, *Sting1*$^{-/-}$L929 cells stably expressing FLAG-STING were transfected with HT-DNA (1 μg/ml) (**h**) or infected with HSV-1 (MOI = 1) (**i**), followed by immunoblotting. Data are presented as means ± s.d. of n = 3 independent biological replicates for **a-d**. P-value was calculated by two-tailed Student's t-test. Data are representative of three independent experiments. Uncropped gel images and numerical data are available in source data.

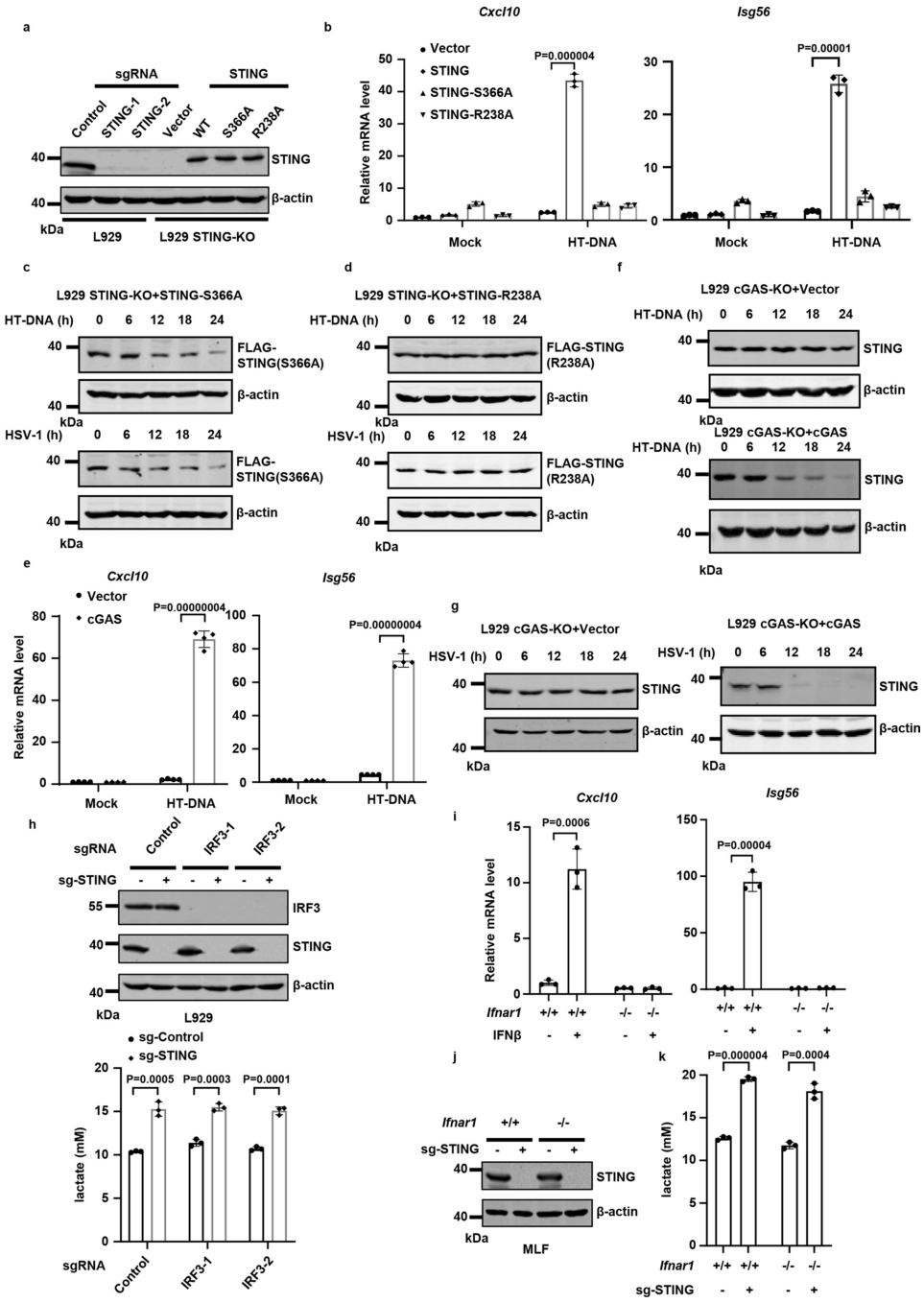

Extended Data Fig. 3 |. STING suppresses lactate production independent of its innate immune function.

a, WT, *Sting1*$^{-/-}$ L929 cells and the reconstituted *Sting1*$^{-/-}$ L929 cells were analysed by immunoblotting. **b**, *Sting1*$^{-/-}$ L929 cells reconstituted with vector control, STING WT or the indicated mutants were stimulated with or without HT-DNA, and *Isg56* or *Cxcl10* mRNA was quantified at 6 h post-stimulation. **c**, immunoblotting analysis of STING-S366A reconstituted *Sting1*$^{-/-}$ L929 cells stimulated with HT-DNA or infected with HSV-1 for the indicated amount of time. **d**, immunoblotting analysis of STING-R238A reconstituted

Sting1$^{-/-}$ L929 cells stimulated with HT-DNA or infected with HSV-1 for the indicated amount of time. **e**, *Cgas*$^{-/-}$ L929 cells reconstituted with vector control or cGAS were stimulated with or without HT-DNA, and *Isg56* and *Cxcl10* mRNA was quantified at 6 h post-stimulation. **f** and **g**, Immunoblotting of the reconstituted *Cgas*$^{-/-}$ L929 cells stimulated with HT-DNA (**f**) or infected with HSV-1 (**g**) for the indicated amount of time. **h**, L929 cells were transduced with control sgRNA or sgRNA targeting IRF3, and the stable cells were further transduced with control sgRNA or sg-STING to generate double knockout cells. WCLs were analysed by immunoblotting and lactate production was measured. **i**, Mouse lung fibroblasts (MLFs) isolated from WT or *Ifnar1*$^{-/-}$ mice were stimulated with or without Interferon-β (IFNβ), and *Cxcl10* or *Isg56* mRNA was quantified by qPCR at 6 h post-stimulation. **j** and **k**, WT and *Ifnar1*$^{-/-}$ MLF cells were transduced with control sgRNA or sg-STING. WCLs were analysed by immunoblotting (**j**) and lactate production was measured (**k**). Data are presented as means ± s.d. of n = 3 independent biological replicates for **b**, **h**, **i**, **k**, and n = 4 independent biological replicates for **e**. P-values were calculated by two-tailed Student's t-test. Data are representative of three independent experiments. Uncropped gel images and numerical data are available in source data.

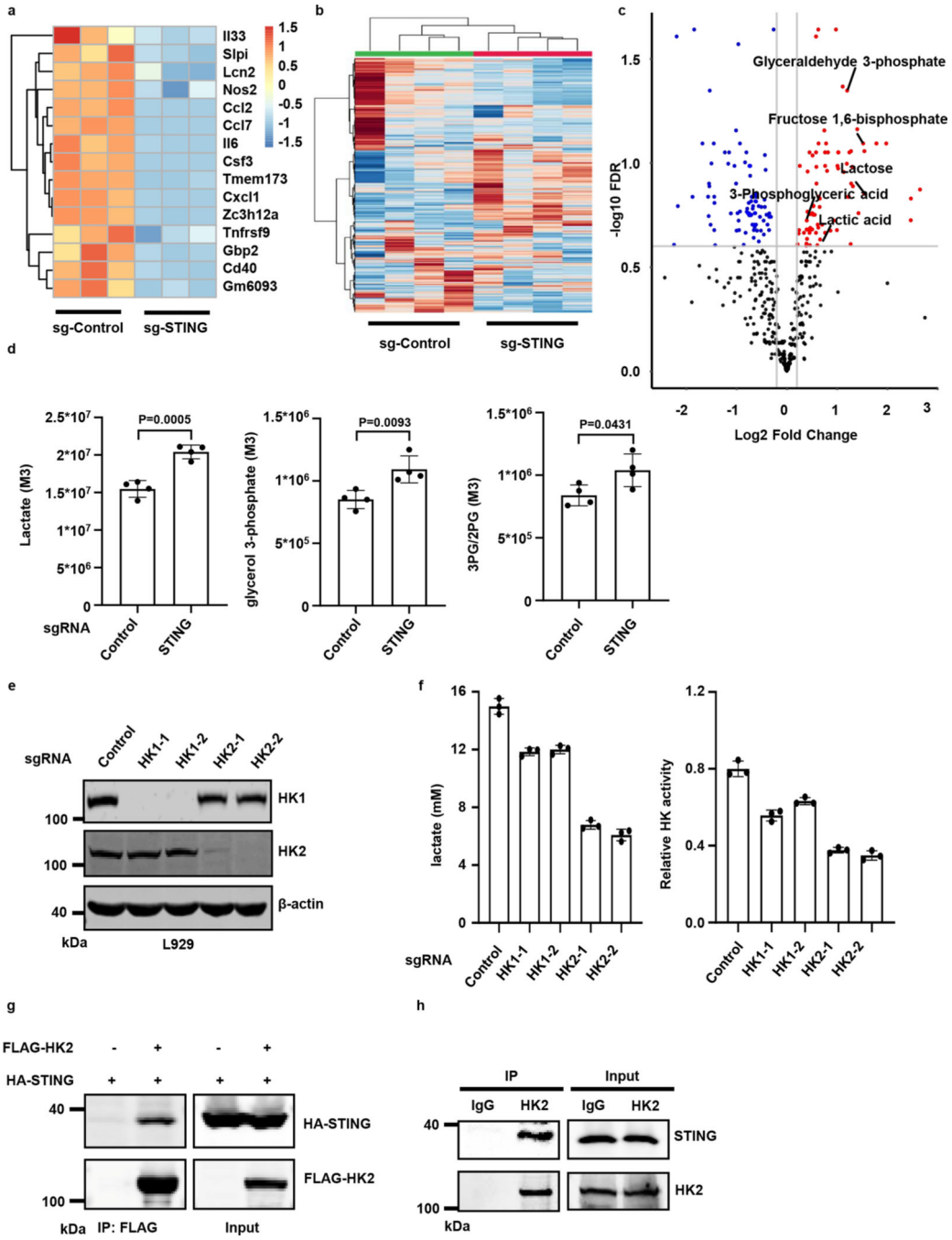

Extended Data Fig. 4 |. STING restricts aerobic glycolysis by targeting HK2.

a, RNA-seq was performed from control and *Sting1*$^{-/-}$ L929 cells. A heatmap shows the top 15 genes down-regulated in *Sting1*$^{-/-}$ L929 cells (n = 3 independent biological replicates). **b**, Heatmap of unsupervised hierarchical clustering of metabolites in control and *Sting1*$^{-/-}$ L929 cells. **c**, A volcano plot visualized metabolites that differ between control and *Sting1*$^{-/-}$ L929 cells, with glycolytic intermediates being annotated. **d**, [U-^{13}C] -glucose stable isotope tracer analyses were performed in control and *Sting1*$^{-/-}$ L929 cells. The M3-labelled glycolysis intermediates (glycerol 3-phosphate, 3PG/2PG, Lactate) were displayed. Four

replicates were analysed per experiment. **e** and **f**, L929 cells were transduced with control sgRNA or sgRNA targeting HK1 or HK2 to generate knockout cells. WCLs were analysed by immunoblotting (**e**), followed by the detection of lactate secretion and mitochondrial hexokinase activity (**f**). **g**, HEK293T cells were transfected with the indicated plasmids. WCLs were collected for immunoprecipitation with anti-FLAG affinity agarose, followed by immunoblotting analysis. **h**, Co-immunoprecipitation and immunoblotting of endogenous STING and HK2 in THP-1 cells. Anti-HK2 antibody was used for immunoprecipitation. Data are presented as means ± s.d. of n = 4 (**d**) or n = 3 (**f**) independent biological replicates. Statistical analyses were performed using a two-tailed unpaired Student's t-test. Data are representative of three independent experiments. Source numerical data and unprocessed blots are provided in Source Data.

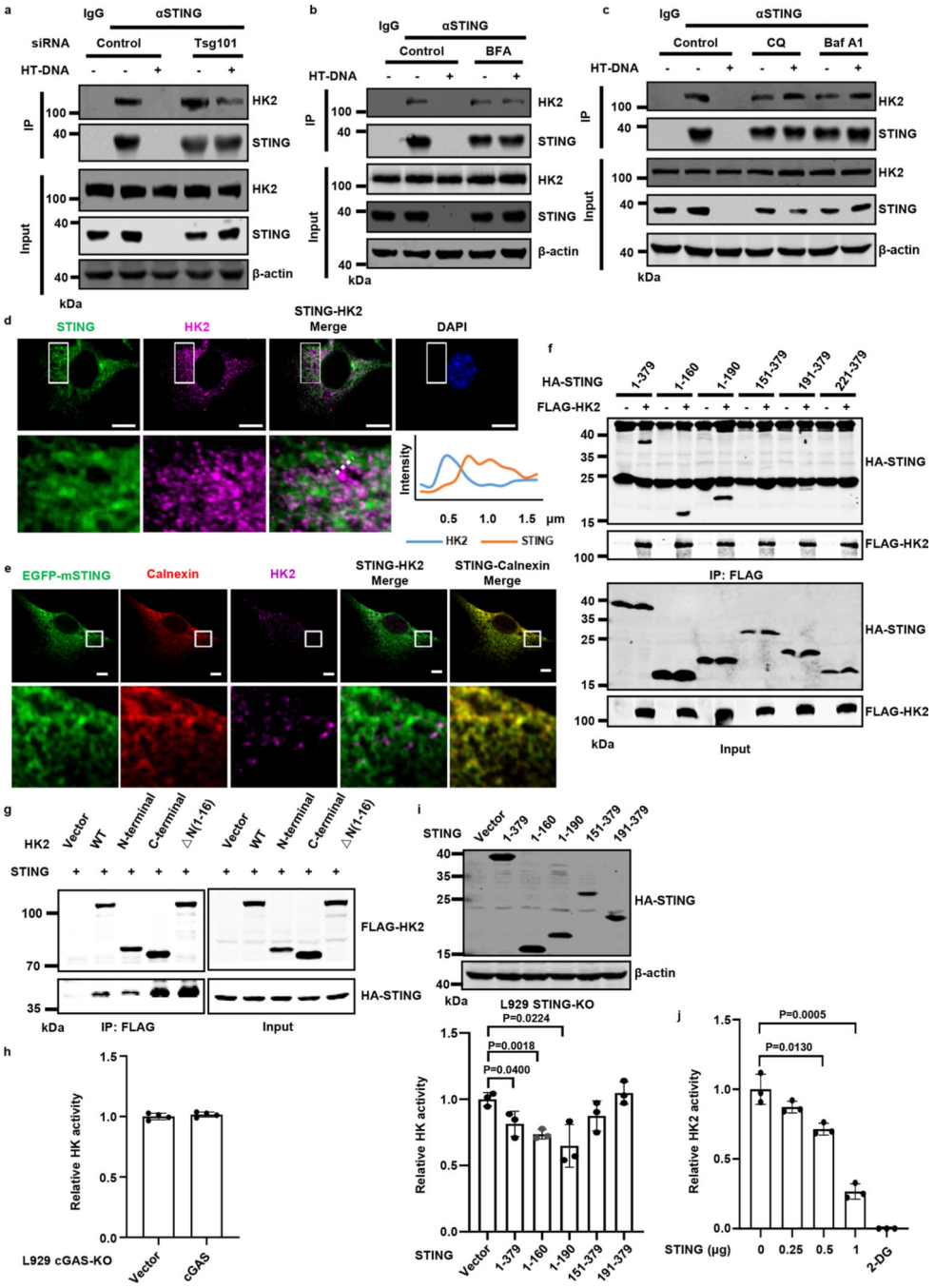

Extended Data Fig. 5 |. STING(1–160) associates with HK2 and suppresses HK2 activity.

a, L929 cells were transfected with control siRNA or *Tsg101* siRNA for 60 h, and then stimulated with HT-DNA (1 μg/ml) for 12 h. Co-immunoprecipitation and immunoblot of endogenous STING and HK2 were shown as indicated. Anti-STING antibody was used for immunoprecipitation. **b** and **c**, L929 cells were pre-treated with brefeldin A (10 μg/ml), chloroquine (20 μM) or bafilomycin A1 (400 nM) for 30 minutes and then stimulated with HT-DNA (1 μg/ml) for 12 h. Co-immunoprecipitation and immunoblotting of endogenous STING and HK2 were shown as indicated. Anti-STING antibody was used

for immunoprecipitation. **d**, the localization of HK2 and STING was visualized in MLF cells. Scale bars, 10 μm. The boxed areas in the top panels were magnified in the bottom, and the fluorescence intensity profile along the white dotted line was shown. **e**, *Sting1*$^{-/-}$ MLF cells stably expressing EGFP-mSTING were immunostained with anti-HK2 and anti-Calnexin (an ER marker) antibodies, and imaged by STED super-resolution microscopy. Scale bars, 5 μm. The boxed areas in the top panels were magnified in the bottom. **f** and **g**, Domain mapping of the interaction between STING and HK2. **h**, Analysis of hexokinase activity in purified mitochondria isolated from control and *Cgas*$^{-/-}$ L929 cells. **i**, *Sting1*$^{-/-}$ L929 cells were reconstituted with the indicated STING mutants, and mitochondrial hexokinase activity was analysed. **j**, Purified GST-HK2 was incubated with the indicated amount of purified STING, followed by the measurement of hexokinase activity. 2-DG (a hexokinase inhibitor) was a positive control. For **h-j**, Data are presented as means ± s.d. of n = 4 (**h**) or n = 3 (**i** and **j**) independent biological replicates. Statistical analyses were performed using a two-tailed unpaired Student's t-test. Data are representative of three independent experiments. Source numerical data and unprocessed blots are provided in Source Data.

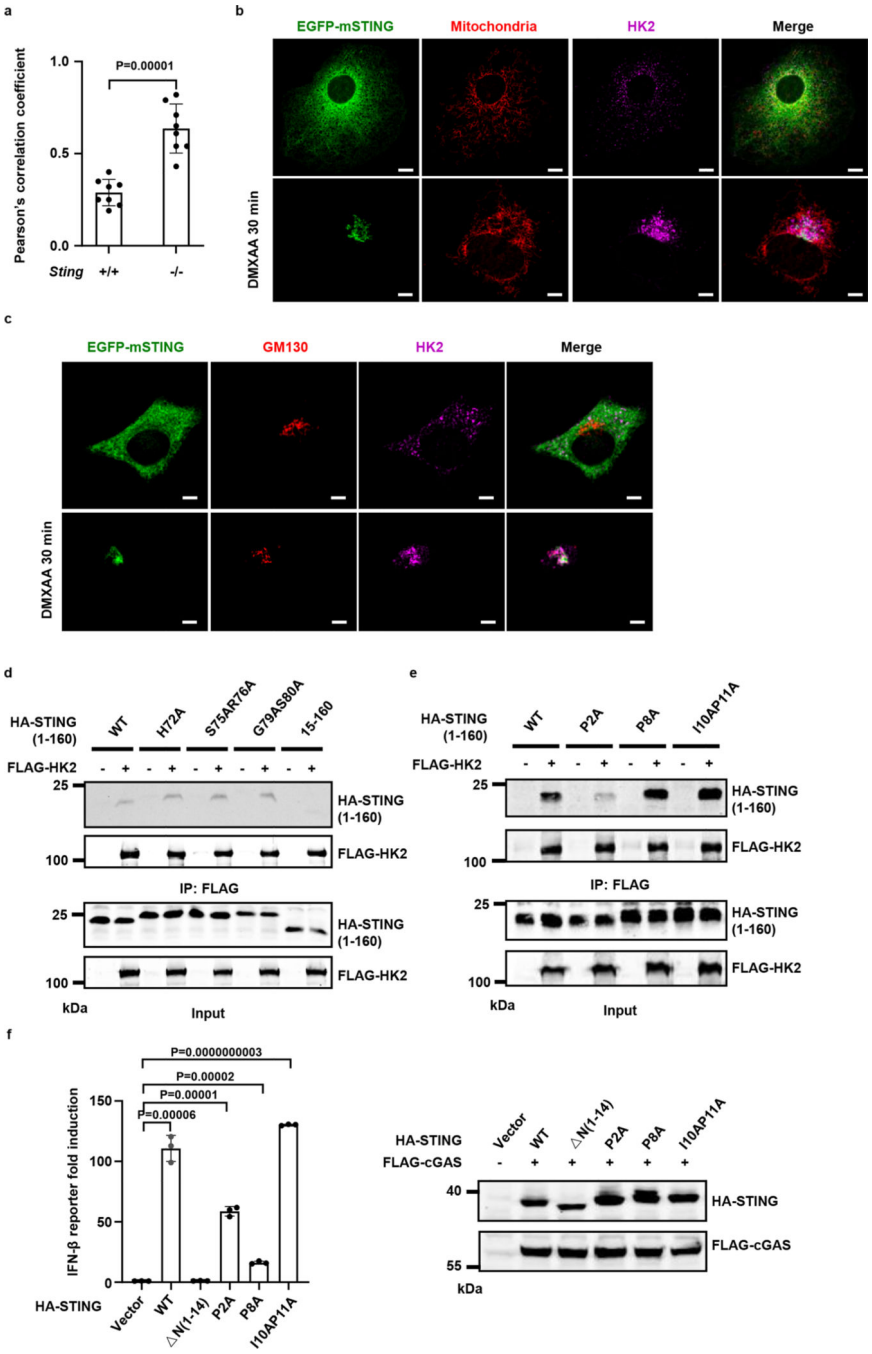

Extended Data Fig. 6 |. P2 of STING is required to associate with HK2 and suppress HK2 activity.

a, The Pearson's correlation coefficients between HK2 and mitochondria. **b**, *Sting1*$^{-/-}$ MLF cells stably expressing EGFP-mSTING were labelled with MitoTracker and stimulated with DMXAA (25 μg/ml) for 30 min. After immunostaining with HK2 antibody, cells were imaged by STED super-resolution microscopy. Scale bars, 5 μm. **c**, *Sting1*$^{-/-}$ MLF cells stably expressing EGFP-mSTING were stimulated with DMXAA (25 μg/ml) for 30 min. After immunostaining with HK2 and GM130 (a Golgi marker) antibodies, cells were

imaged by STED super-resolution microscopy. Scale bars, 5 μm. **d** and **e**, FLAG-HK2 and HA-tagged STING (1–160) or the indicated mutants were co-expressed in HEK293T cells. WCLs were immunoprecipitated with anti-FLAG agarose and analysed by immunoblotting. **f**, Reporter assays for *IFNB1* promoter activity in HEK293T cells transfected with HA-tagged STING containing the indicated mutations and FLAG-cGAS (Left). WCLs were analysed by immunoblotting (Right). Data are presented as means ± s.d. of n = 8 (**a**) or n = 3 (**f**) independent biological replicates. Statistical analyses were performed using a two-tailed unpaired Student's t-test. Data are representative of three independent experiments. Source numerical data and unprocessed blots are provided in Source Data.

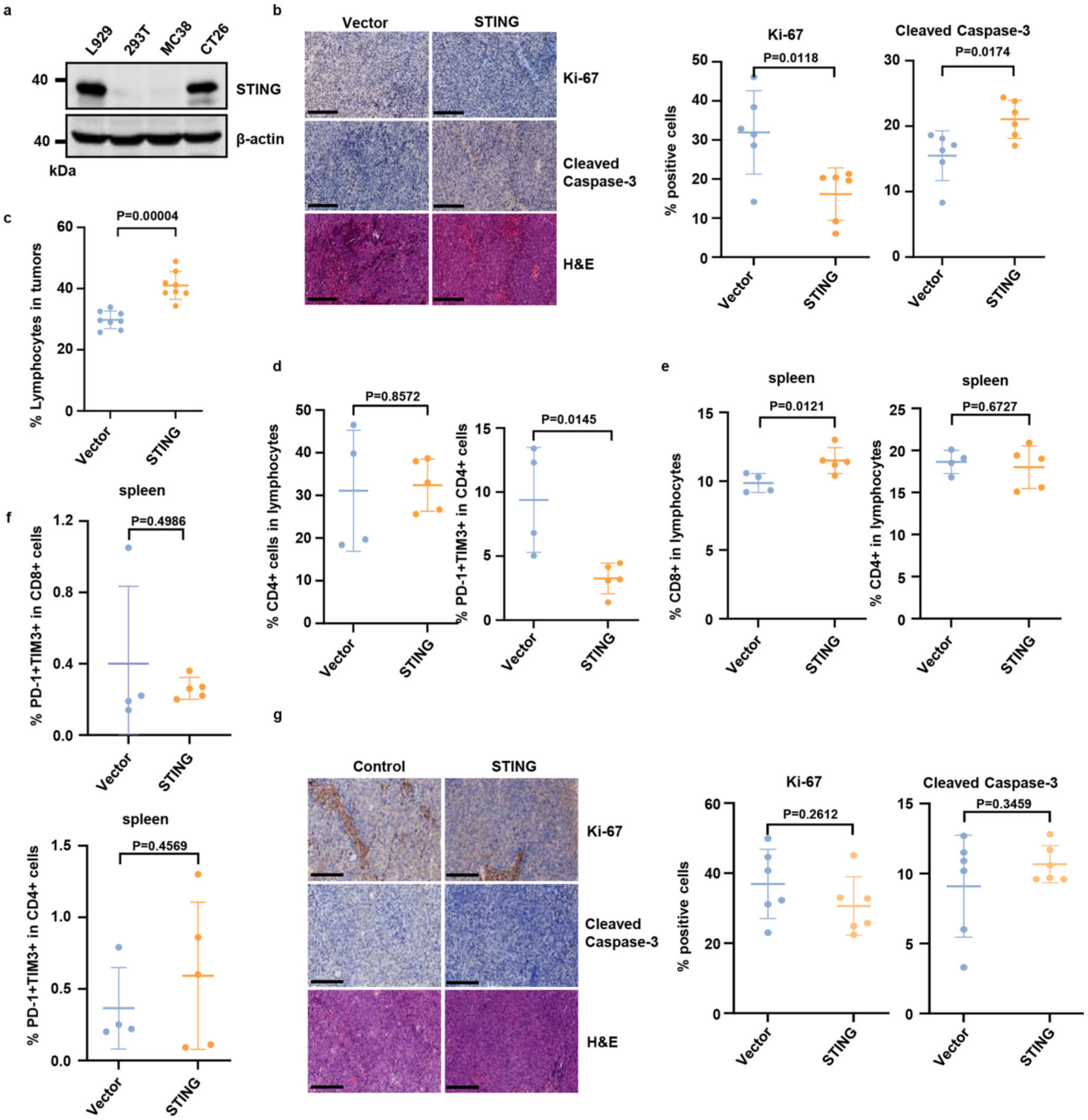

Extended Data Fig. 7 |. STING stable expression in MC38 cells promotes antitumour immunity. **a**, WCLs from L929, 293T, MC38, CT26 were analysed by immunoblotting. **b**, Representative MC38 tumour staining of Ki-67 and cleaved caspase-3 as described in Fig. 5b. The percentage of Ki-67- or cleaved caspase-3-positive cells was quantified (n = 6). Scale bars, 200 μm. **c**, Flow cytometry analysis of lymphocyte in MC38 tumours as described in Fig. 5b (n = 8). **d**, Flow cytometry analysis of tumour-infiltrating $CD4^+$ T cells and the severely exhausted $CD4^+$ cells in MC38 tumours as described in Fig. 5e (n = 4 Vector group, n = 5 STING group). **e** and **f**, Flow cytometry analysis of $CD8^+$ and $CD4^+$ T

cells in the spleens of the MC38 tumour-bearing mice as described in Fig. 5e (n = 4 Vector group, n = 5 STING group). **g**, Representative MC38 tumour-bearing in NSG mice staining of Ki-67 and cleaved caspase-3 as described in Fig. 5f. The percentage of Ki-67- or cleaved caspase-3-positive cells was quantified (n = 6). Scale bars, 200 μm. Data are presented as means ± s.d., and statistical analyses were performed using a two-tailed unpaired Student's t-test. Data are representative of three independent experiments. Source numerical data and unprocessed blots are provided in Source Data.

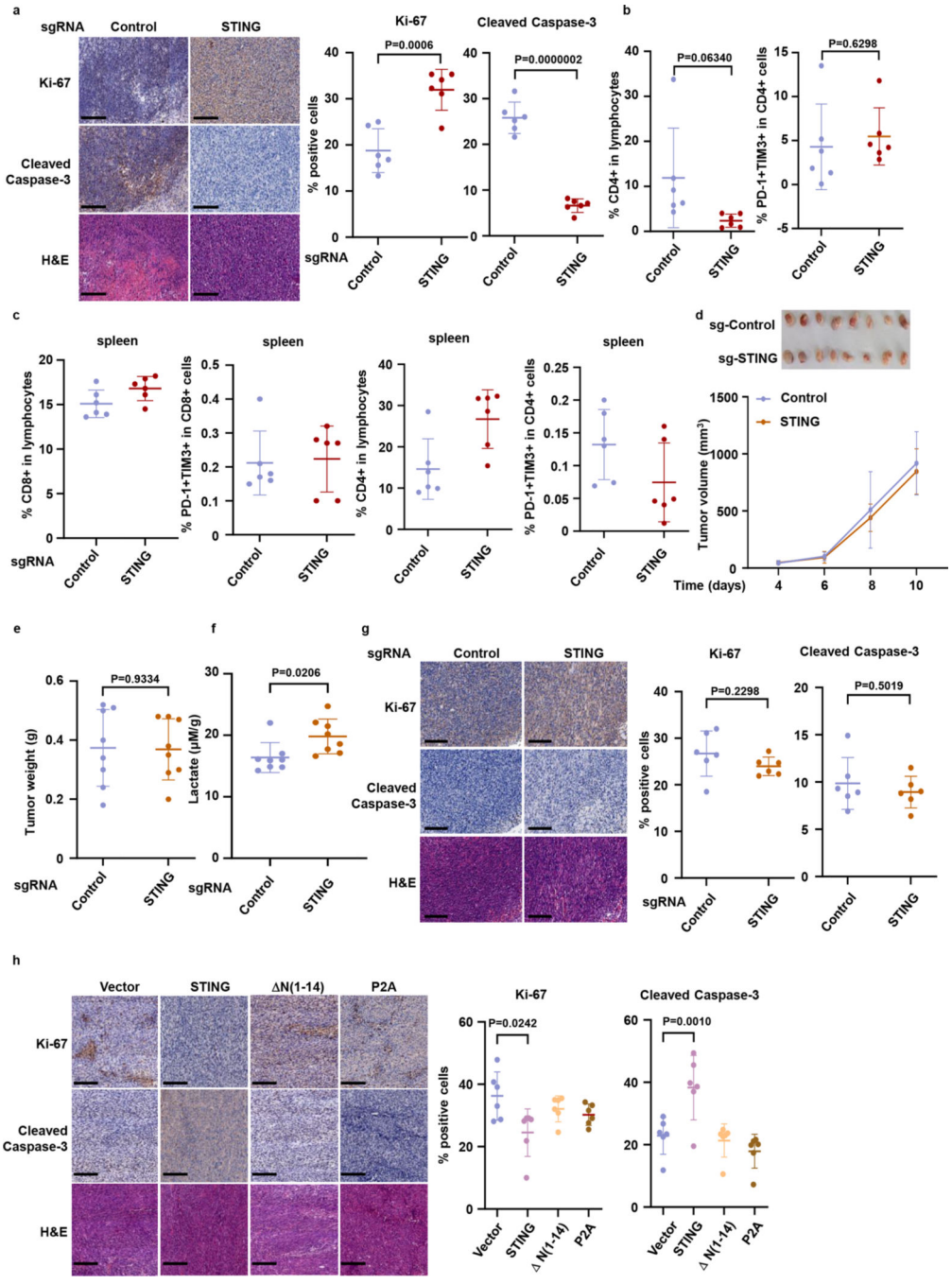

Extended Data Fig. 8 |. Depletion of STING in CT26 cells impairs antitumour immunity.
a, Representative CT26 tumour staining of Ki-67 and cleaved caspase-3 as described in Fig. 5k. The percentage of Ki-67- or cleaved caspase-3-positive cells was quantified (n = 6). Scale bars, 200 μm. **b**, Flow cytometry analysis of the tumour-infiltrating $CD4^+$ T cells and the severe exhausted $CD4^+$ T cells isolated from CT26 tumour and spleens as described in Fig. 5k (n = 6). **c**, Flow cytometry analysis of $CD8^+$ and $CD4^+$ T cells in the spleens of the CT26 tumour-bearing mice (n = 6). **d-g**, CT26 cells as described in Fig. 5i were subcutaneously transplanted into NSG mice (n = 8 per group). Tumour volume (**d**), weight (**e**), and lactate levels in the tumours at 10 days post-transplantation (**f**) were measured. IHC staining of Ki-67 and cleaved caspase-3 of the tumours were shown in (**g**). The percentage of Ki-67- or cleaved caspase-3-positive cells was quantified (n = 6). Scale bars, 200 μm. **h**, IHC staining of Ki-67 and cleaved caspase-3 of MC38 tumour as described in Fig. 5o. The percentage of Ki-67- or cleaved caspase-3-positive cells was quantified (n = 6). Scale bars, 200 μm. Data are presented as means ± s.d., and statistical analyses were performed using a two-tailed unpaired Student's t-test. Data are representative of three independent experiments. Source numerical data and unprocessed blots are provided in Source Data.

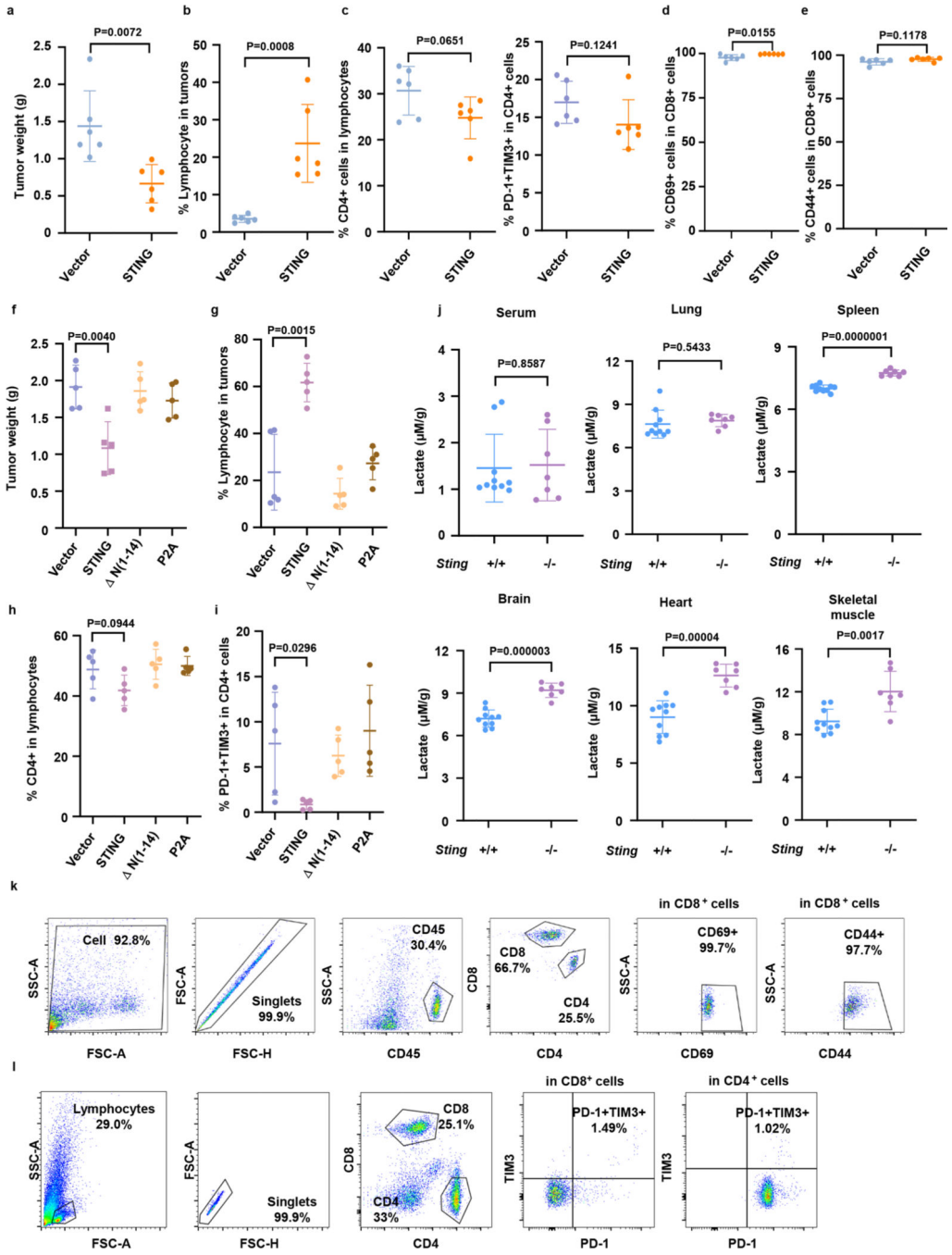

Extended Data Fig. 9 |. STING restricts aerobic glycolysis and promotes antitumour immunity in established tumours.

a, the weight of the tumours at 14 days post-transplantation as described in Fig. 6b was shown (n = 6 in each group). **b**, Flow cytometry analysis of tumour-infiltrating lymphocytes in MC38 tumours as described in Fig. 6b (n = 6). **c**, Flow cytometry analysis of tumour-infiltrating $CD4^+$ T cells and the severe exhausted $CD4^+$ cells in MC38 tumours as described in Fig. 6b (n = 6). **d** and **e**, Flow cytometry analysis of $CD69^+$ (**d**) or $CD44^+$ (**e**) cells in tumour-infiltrating $CD8^+$ cells in MC38 tumours as described in Fig. 6b (n = 6). **f**, the

weight of the tumours at 16 days post-transplantation as described in Fig. 6g was shown (n = 5). **g**, Flow cytometry analysis of lymphocytes in MC38 tumours as described in Fig. 6g (n = 5). **h and i**, Flow cytometry analysis of tumour-infiltrating $CD4^+$ T cells in lymphocytes (**h**) and the severely exhausted $CD4^+$ T cells (**i**) in MC38 tumours as described in Fig. 6g (n = 5). **j**, Measurement of lactate levels in serum, lung, spleen, brain, heart and skeletal muscle of *Sting1*$^{+/+}$ and *Sting1*$^{-/-}$ mice (n = 10 in *Sting1*$^{+/+}$ group and n = 7 in *Sting1*$^{-/-}$ group). **k** and **l**, representative figures showing gating strategies for all flow cytometry analysis in this study. Data are presented as means ± s.d., and statistical analyses were performed using a two-tailed unpaired Student's t-test. Data are representative of three independent experiments. Source numerical data and unprocessed blots are provided in Source Data.

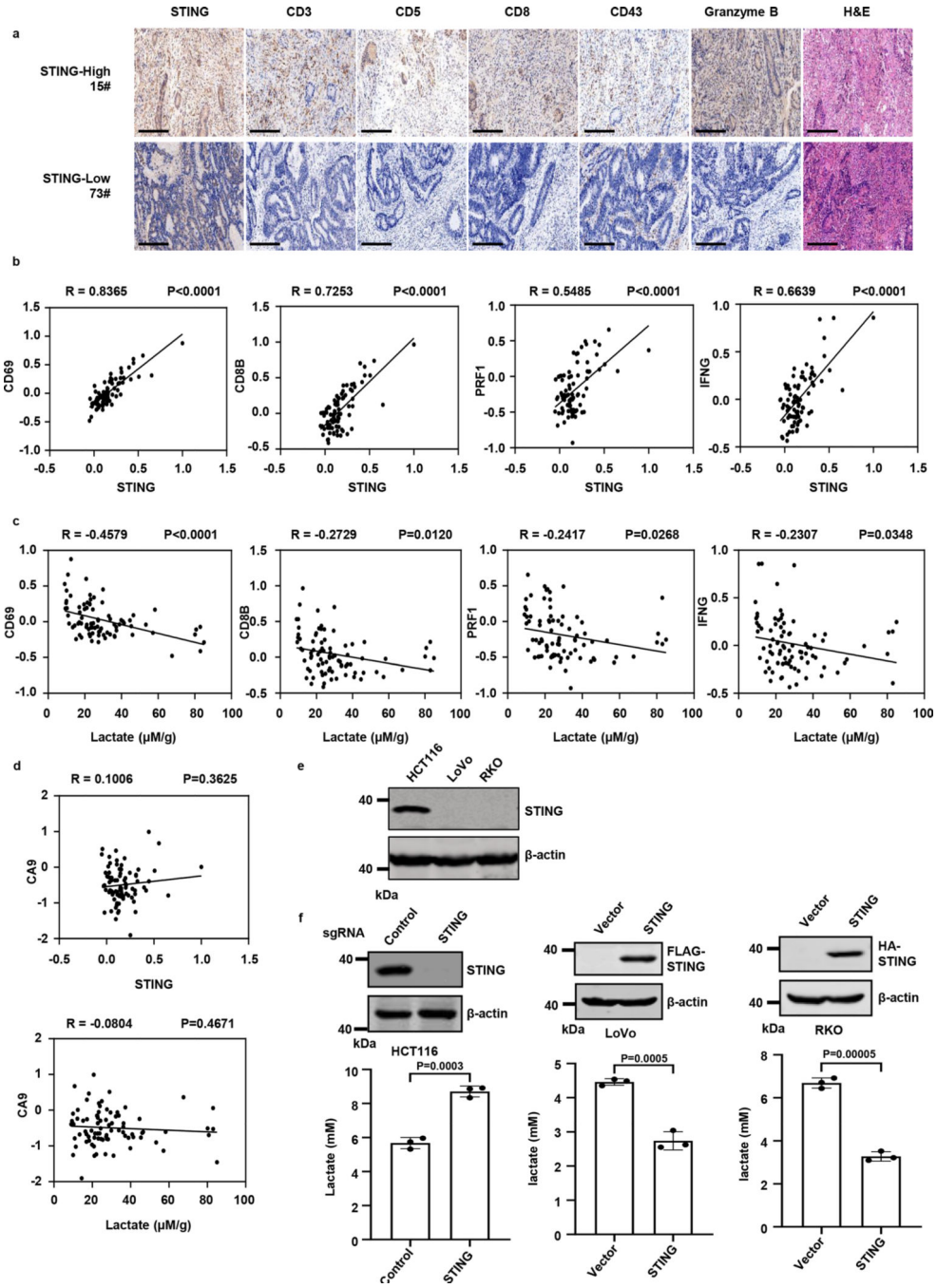

Extended Data Fig. 10 |. STING restricts aerobic glycolysis in CRC tissues and human CRC cell lines.

a, Representative IHC staining of tumour tissue in human colorectal carcinomas. Scale bar, 200 μm. **b**, Correlations between the STING levels and the expression of the indicated markers in colorectal tumour tissue (n = 84). **c**, Correlations between the lactate levels and the expression of the indicated markers in colorectal tumour tissue (n = 84). **d**, Correlations between the STING or lactate levels and the expression of CA9 in colorectal tumour tissue (n = 84). **e**, WCLs from HCT116, LoVo and RKO cells were analysed by immunoblotting.

f, HCT116 cells were transduced with sgRNA targeting STING to generate knockout cells, while LoVo and RKO cells were transduced to stably express STING. WCLs were analysed by immunoblotting, and lactate levels were quantified (n = 3 biological repeats). Data are presented as means ± s.d., and statistical analyses were performed using a two-tailed unpaired Student's t-test for **f**. A two-sided Pearson's chi-squared test was performed for **b**–**d**. Data are representative of three independent experiments. Source numerical data and unprocessed blots are provided in Source Data.

Supplementary Material

Refer to Web version on PubMed Central for supplementary material.

Acknowledgements

We thank J. Zhang, Q. Yang, B. Zhong, H. Liu, C. Cai, W. Song, H. Du, Z. J. Chen and X. Zhou for reagents; B. Zhong for suggestions; and the members of the core facility of the Medical Research Institute at Wuhan University for technical support. This work was supported by the National Key Research and Development Program of China 2021YFC2701800 (to J.Z.), 2021YFC2701804 (to J.Z.) and 2021YFC2701602 (to B.W.); a startup fund from Wuhan University (to J.Z.); National Natural Science Foundation of China 31970156 (to J.Z.), 82172261 (to J.Z.), 32188101 (to H.-B.S.) and 32170886 (to B.W.); the Fundamental Research Funds for the Central Universities (2042022dx0003) (to J.Z.) and 2042022rc0032 (to B.W.); and the Non-Profit Central Research Institute Fund of Chinese Academy of Medical Sciences 2020-PT320-004 (to J.Z.). The funders had no role in study design, data collection and analysis, decision to publish or preparation of the manuscript.

Data availability

RNA-seq data supporting the findings of this study have been deposited in the Gene Expression Omnibus under accession code GSE202637. All other data supporting the findings of this study are available from the corresponding author on reasonable request. Source data are provided with this paper.

References

1. Glickman LH et al. Direct activation of STING in the tumor microenvironment leads to potent and systemic tumor regression and immunity. Cancer Res. 76, 1018–1030 (2016).
2. Woo SR et al. STING-dependent cytosolic DNA sensing mediates innate immune recognition of immunogenic tumors. Immunity 41, 830–842 (2014). [PubMed: 25517615]
3. Zhang Z-D & Zhong B. Regulation and function of the cGAS-MITA/STING axis in health and disease. Cell Insight 1, 100001 (2022). [PubMed: 37192983]
4. Yum S, Li MH, Frankel AE & Chen ZJJ Roles of the cGAS-STING pathway in cancer immunosurveillance and immunotherapy. Annu. Rev. Cancer Biol 3, 323–344 (2019).
5. Kwon J. & Bakhoum SF The cytosolic DNA-sensing cGAS-STING pathway in cancer. Cancer Discov. 10, 26–39 (2020). [PubMed: 31852718]
6. Sun LJ, Wu JX, Du FH, Chen X. & Chen ZJJ Cyclic GMP-AMP synthase is a cytosolic DNA sensor that activates the type I interferon pathway. Science 339, 786–791 (2013). [PubMed: 23258413]
7. Wu JX et al. Cyclic GMP-AMP is an endogenous second messenger in innate immune signaling by cytosolic DNA. Science 339, 826–830 (2013). [PubMed: 23258412]
8. Zhong B. et al. The adaptor protein MITA links virus-sensing receptors to IRF3 transcription factor activation. Immunity 29, 538–550 (2008). [PubMed: 18818105]
9. Ishikawa H. & Barber GN STING is an endoplasmic reticulum adaptor that facilitates innate immune signalling. Nature 455, 674–678 (2008). [PubMed: 18724357]

10. Wang H. et al. cGAS is essential for the antitumor effect of immune checkpoint blockade. Proc. Natl Acad. Sci USA 114, 1637–1642 (2017). [PubMed: 28137885]
11. Liu W. et al. Selective reactivation of STING signaling to target Merkel cell carcinoma. Proc. Natl Acad. Sci. USA 117, 13730–13739 (2020). [PubMed: 32482869]
12. Song SS et al. Decreased expression of STING predicts poor prognosis in patients with gastric cancer. Sci. Rep. 7, 39858 (2017). [PubMed: 28176788]
13. Xia T, Konno H, Ahn J. & Barber GN Deregulation of STING signaling in colorectal carcinoma constrains DNA damage responses and correlates with tumorigenesis. Cell Rep. 14, 282–297 (2016). [PubMed: 26748708]
14. Kitajima S. et al. Suppression of STING associated with LKB1 loss in KRAS-driven lung cancer. Cancer Discov. 9, 34–45 (2019). [PubMed: 30297358]
15. Xia T, Konno H. & Barber GN Recurrent loss of STING signaling in melanoma correlates with susceptibility to viral oncolysis. Cancer Res. 76, 6747–6759 (2016). [PubMed: 27680683]
16. Falahat R. et al. STING signaling in melanoma cells shapes antigenicity and can promote antitumor T-cell activity. Cancer Immunol. Res. 7, 1837–1848 (2019). [PubMed: 31462408]
17. Gatenby RA & Gillies RJ Why do cancers have high aerobic glycolysis? Nat. Rev. Cancer 4, 891–899 (2004). [PubMed: 15516961]
18. Lim AR, Rathmell WK & Rathmell JC The tumor microenvironment as a metabolic barrier to effector T cells and immunotherapy. eLife 9, e55185 (2020). [PubMed: 32367803]
19. Reinfeld BI, Rathmell WK, Kim TK & Rathmell JC The therapeutic implications of immunosuppressive tumor aerobic glycolysis. Cell. Mol. Immunol. 19, 46–58 (2021). [PubMed: 34239083]
20. Brand A. et al. LDHA-associated lactic acid production blunts tumor immunosurveillance by T and NK Cells. Cell Metab. 24, 657–671 (2016). [PubMed: 27641098]
21. Colegio OR et al. Functional polarization of tumour-associated macrophages by tumour-derived lactic acid. Nature 513, 559–563 (2014). [PubMed: 25043024]
22. Gui X. et al. Autophagy induction via STING trafficking is a primordial function of the cGAS pathway. Nature 567, 262–266 (2019). [PubMed: 30842662]
23. Gonugunta VK et al. Trafficking-mediated STING degradation requires sorting to acidified endolysosomes and can be targeted to enhance anti-tumor response. Cell Rep. 21, 3234–3242 (2017). [PubMed: 29241549]
24. An J, Woodward JJ, Sasaki T, Minie M. & Elkon KB Cutting edge: antimalarial drugs inhibit IFN-β production through blockade of cyclic GMP-AMP synthase-DNA interaction. J. Immunol 194, 4089–4093 (2015). [PubMed: 25821216]
25. Mukai K. et al. Activation of STING requires palmitoylation at the Golgi. Nat. Commun. 7, 11932 (2016). [PubMed: 27324217]
26. Kuchitsu Y. et al. STING signalling is terminated through ESCRT-dependent microautophagy of vesicles originating from recycling endosomes. Nat. Cell Biol 25, 453–466 (2023). [PubMed: 36918692]
27. Sun X. et al. DNA-PK deficiency potentiates cGAS-mediated antiviral innate immunity. Nat. Commun. 11, 6182 (2020). [PubMed: 33273464]
28. Liu S. et al. Phosphorylation of innate immune adaptor proteins MAVS, STING, and TRIF induces IRF3 activation. Science 347, aaa2630 (2015).
29. Schoggins JW et al. Pan-viral specificity of IFN-induced genes reveals new roles for cGAS in innate immunity. Nature 505, 691–695 (2014). [PubMed: 24284630]
30. Bansal A. & Simon MC Glutathione metabolism in cancer progression and treatment resistance. J. Cell Biol 217, 2291–2298 (2018). [PubMed: 29915025]
31. Mattaini KR, Sullivan MR & Vander Heiden MG The importance of serine metabolism in cancer. J. Cell Biol 214, 249–257 (2016). [PubMed: 27458133]
32. Mukai K. et al. Homeostatic regulation of STING by retrograde membrane traffic to the ER. Nat. Commun. 12, 61 (2021). [PubMed: 33397928]
33. Deng Z. et al. A defect in COPI-mediated transport of STING causes immune dysregulation in COPA syndrome. J. Exp. Med. 217, e20201045 (2020).

34. DeWaal D. et al. Hexokinase-2 depletion inhibits glycolysis and induces oxidative phosphorylation in hepatocellular carcinoma and sensitizes to metformin. Nat. Commun 9, 446 (2018). [PubMed: 29386513]
35. Roberts DJ & Miyamoto S. Hexokinase II integrates energy metabolism and cellular protection: Akting on mitochondria and TORCing to autophagy. Cell Death Differ. 22, 248–257 (2015). [PubMed: 25323588]
36. Ciscato F. et al. Hexokinase 2 displacement from mitochondria-associated membranes prompts Ca^{2+}-dependent death of cancer cells. EMBO Rep. 21, e49117 (2020). [PubMed: 32383545]
37. Zhang W. et al. Lactate is a natural suppressor of RLR signaling by targeting MAVS. Cell 178, 176–189 (2019). [PubMed: 31155231]
38. Rath A, Glibowicka M, Nadeau VG, Chen G. & Deber CM Detergent binding explains anomalous SDS-PAGE migration of membrane proteins. Proc. Natl Acad. Sci. USA 106, 1760–1765 (2009). [PubMed: 19181854]
39. Shang G, Zhang C, Chen ZJ, Bai XC & Zhang X. Cryo-EM structures of STING reveal its mechanism of activation by cyclic GMP-AMP. Nature 567, 389–393 (2019). [PubMed: 30842659]
40. Patra KC et al. Hexokinase 2 is required for tumor initiation and maintenance and its systemic deletion is therapeutic in mouse models of cancer. Cancer Cell 24, 213–228 (2013). [PubMed: 23911236]
41. Pastorekova S. & Gillies RJ The role of carbonic anhydrase IX in cancer development: links to hypoxia, acidosis, and beyond. Cancer Metastasis Rev. 38, 65–77 (2019). [PubMed: 31076951]
42. Swietach P, Patiar S, Supuran CT, Harris AL & Vaughan-Jones RD The role of carbonic anhydrase 9 in regulating extracellular and intracellular pH in three-dimensional tumor cell growths. J. Biol. Chem. 284, 20299–20310 (2009). [PubMed: 19458084]
43. Patel S. & Jin L. *TMEM173* variants and potential importance to human biology and disease. Genes Immun. 20, 82–89 (2019). [PubMed: 29728611]
44. Hamann L. et al. STING SNP R293Q is associated with a decreased risk of aging-related diseases. Gerontology 65, 145–154 (2019). [PubMed: 30368497]
45. Falahat R. et al. Epigenetic reprogramming of tumor cell-intrinsic STING function sculpts antigenicity and T cell recognition of melanoma. Proc. Natl Acad. Sci. USA 118, e2013598118 (2021).
46. Amouzegar A, Chelvanambi M, Filderman JN, Storkus WJ & Luke JJ STING agonists as cancer therapeutics. Cancers 13, 2695 (2021). [PubMed: 34070756]
47. Le Naour J, Zitvogel L, Galluzzi L, Vacchelli E. & Kroemer G. Trial watch: STING agonists in cancer therapy. Oncoimmunology 9, 1777624 (2020).
48. Akhmetova K, Balasov M. & Chesnokov I. Drosophila STING protein has a role in lipid metabolism. eLife 10, e67358 (2021). [PubMed: 34467853]
49. Jiang H. et al. Chromatin-bound cGAS is an inhibitor of DNA repair and hence accelerates genome destabilization and cell death. EMBO J. 38, e102718 (2019).
50. Chen H. et al. cGAS suppresses genomic instability as a decelerator of replication forks. Sci. Adv. 6, eabb8941 (2020).
51. Liu HP et al. Nuclear cGAS suppresses DNA repair and promotes tumorigenesis. Nature 563, 131–136 (2018). [PubMed: 30356214]
52. Contreras-Baeza Y. et al. Monocarboxylate transporter 4 (MCT4) is a high affinity transporter capable of exporting lactate in high-lactate microenvironments. J. Biol. Chem. 294, 20135–20147 (2019). [PubMed: 31719150]
53. Dobbs N. et al. STING activation by translocation from the ER is associated with infection and autoinflammatory disease. Cell Host Microbe 18, 157–168 (2015). [PubMed: 26235147]
54. Liu Y. et al. Clathrin-associated AP-1 control stermination of STING signalling. Nature 610, 761–767 (2022). [PubMed: 36261523]
55. Zhang J. et al. Species-specific deamidation of cGAS by herpes simplex virus UL37 protein facilitates viral replication. Cell Host Microbe 24, 234–248 (2018). [PubMed: 30092200]
56. Luo WW et al. iRhom2 is essential for innate immunity to DNA viruses by mediating trafficking and stability of the adaptor STING. Nat. Immunol. 17, 1057–1066 (2016). [PubMed: 27428826]

57. Zhang JJ et al. IκB kinase ε is an NFATc1 kinase that inhibits T cell immune response. Cell Rep. 16, 405–418 (2016). [PubMed: 27346349]

58. Minassian A. et al. An internally translated MAVS variant exposes its amino-terminal TRAF-binding motifs to deregulate interferon induction. PLoS Pathog. 11, e1005060 (2015).

59. Wang Y. et al. Coordinative metabolism of glutamine carbon and nitrogen in proliferating cancer cells under hypoxia. Nat. Commun. 10, 201 (2019). [PubMed: 30643150]

60. Wen B, Mei ZL, Zeng CW & Liu SQ metaX: a flexible and comprehensive software for processing metabolomics data. BMC Bioinform. 18, 183 (2017).

61. Zhang JJ et al. Herpesviral G protein-coupled receptors activate NFAT to induce tumor formation via inhibiting the SERCA calcium ATPase. PLoS Pathog. 11, e1004768 (2015).

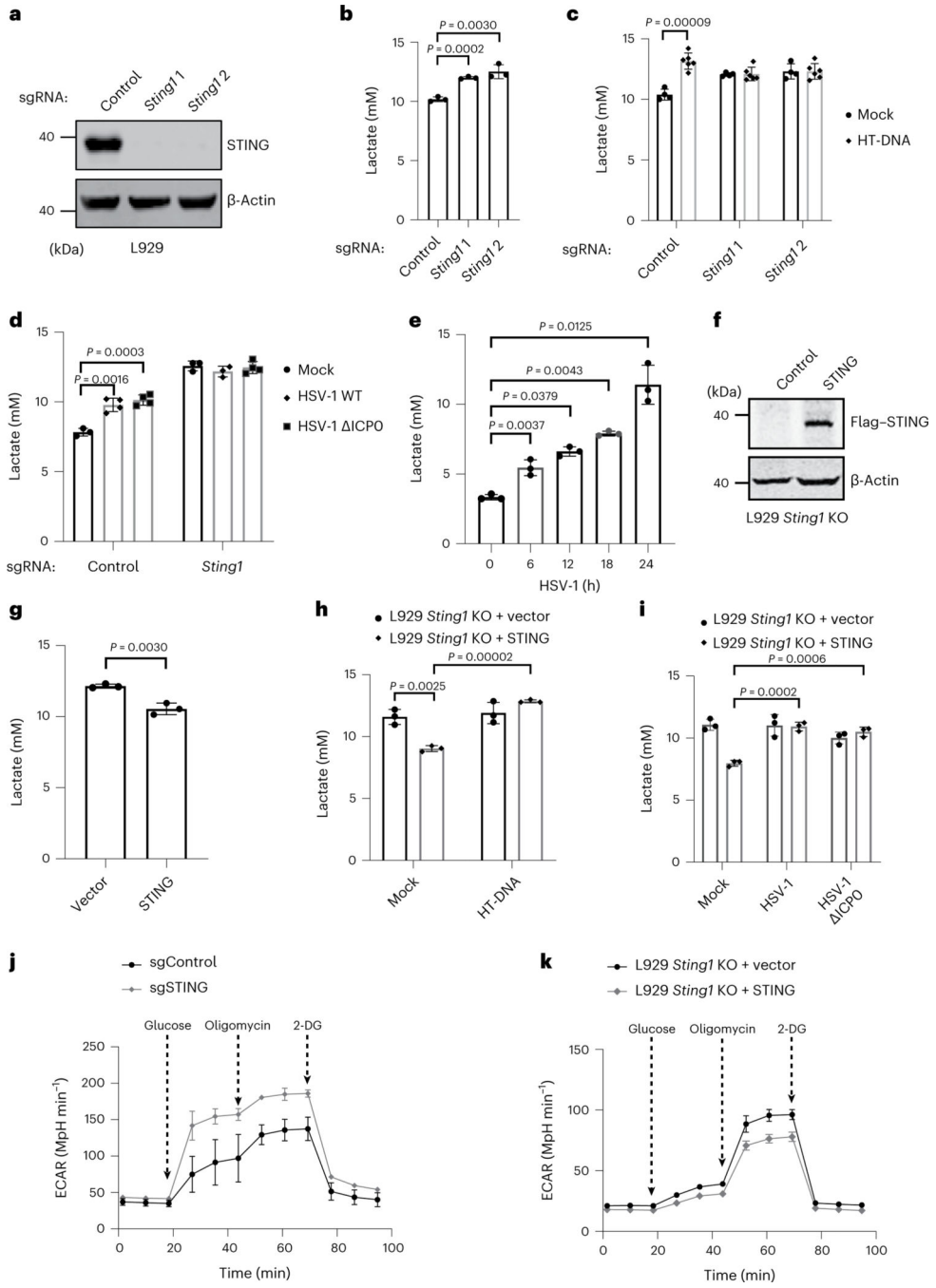

Fig. 1 |. STING suppresses aerobic glycolysis.

a, L929 cells were transduced with single guide RNA (sgRNA) targeting *Sting1* to generate KO cells. Whole-cell lysates (WCLs) were analysed by immunoblotting. **b**, Measurement of lactate levels in control or *Sting1*$^{-/-}$ L929 cells. **c**, Control or *Sting1*$^{-/-}$ L929 cells were transfected with or without HT-DNA (1 μg ml^{-1}), and lactate was measured at 24 h after transfection. From left to right, n = 4, 6, 4, 6, 4 and 6 biologically independent samples. **d**, Control or *Sting1*$^{-/-}$ L929 cells were infected with HSV-1 WT or ΔICP0 (ICP0-deficient) (multiplicity of infection (MOI) = 1), and lactate was measured at 24 h after infection. From

left to right, n = 3, 4, 4, 3, 3 and 4 biologically independent samples. **e**, THP-1 cells were infected with HSV-1 (MOI = 1), and lactate was measured at the indicated timepoints. **f**, *Sting1*$^{-/-}$ L929 cells were infected with control lentivirus or lentivirus containing STING. WCLs were analysed by immunoblotting. **g**, Measurement of lactate levels of the stable cells as described in **f**. **h**, L929 stable cells as described in **f** were stimulated with or without HT-DNA, and lactate was measured at 24 h after transfection. **i**, L929 stable cells as described in **f** were infected with HSV-1 or ΔICP0 virus (MOI = 1), and lactate was measured at 24 h after infection. **j**,**k**, Measurement of the ECAR in control or *Sting1*$^{-/-}$ L929 cells (**j**) or *Sting1*$^{-/-}$ L929 cells transduced with vector or STING (**k**). Data are mean ± s.d. P values were calculated using two-tailed Student's t-tests. Data are representative of three independent experiments. For **b**, **e** and **g**–**i**, data are from n = 3 independent biological replicates. Uncropped gel images and numerical data are provided as Source Data.

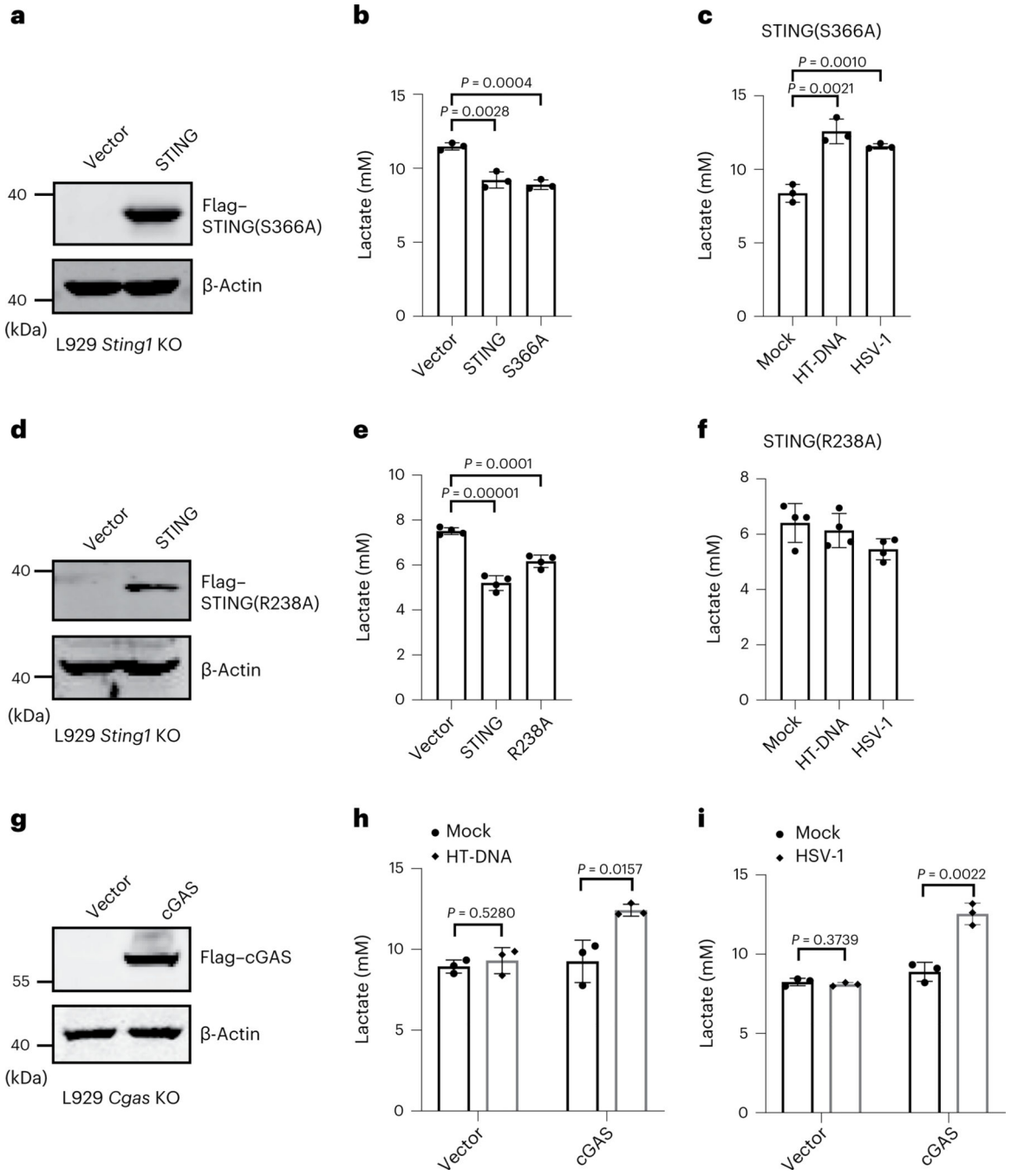

Fig. 2 |. STING suppresses the production of lactate independent of its innate immune function.
a, *Sting1*$^{-/-}$ L929 cells were infected with control (vector) lentivirus or lentivirus containing the indicated STING mutant (S366A). WCLs were analysed by immunoblotting. **b**, Measurement of lactate secretion in *Sting1*$^{-/-}$ L929 cells stably expressing empty vector, WT STING or STING(S366A). **c**, *Sting1*$^{-/-}$ L929 cells stably expressing STING(S366A) were transfected with HT-DNA or infected with HSV-1 for 24 h, and lactate levels were detected. **d**, *Sting1*$^{-/-}$ L929 cells were infected with control (vector) lentivirus or that containing the STING(R238A) mutant. WCLs were analysed using immunoblotting. **e**,

Measurement of lactate secretion in *Sting1*$^{-/-}$ L929 cells stably expressing vector control, WT STING or STING(R238A). **f**, *Sting1*$^{-/-}$ L929 cells stably expressing STING(R238A) were transfected with HT-DNA or infected with HSV-1 for 24 h, and lactate secretion was measured. **g**, *Cgas*$^{-/-}$ L929 cells were transduced with lentivirus expressing vector control or cGAS and analysed using immunoblotting. **h**,**i**, *Cgas*$^{-/-}$ L929 cells stably expressing vector or Flag–cGAS were stimulated with HT-DNA (**h**) or infected with HSV-1 (**i**) for 24 h, and lactate secretion was measured. Data are mean ± s.d. of $n = 3$ independent biological replicates (**b**, **c**, **h** and **i**) and $n = 4$ independent biological replicates (**e** and **f**). *P* values were calculated using two-tailed Student's *t*-tests. Data are representative of three independent experiments. Uncropped gel images and numerical data are provided as Source Data.

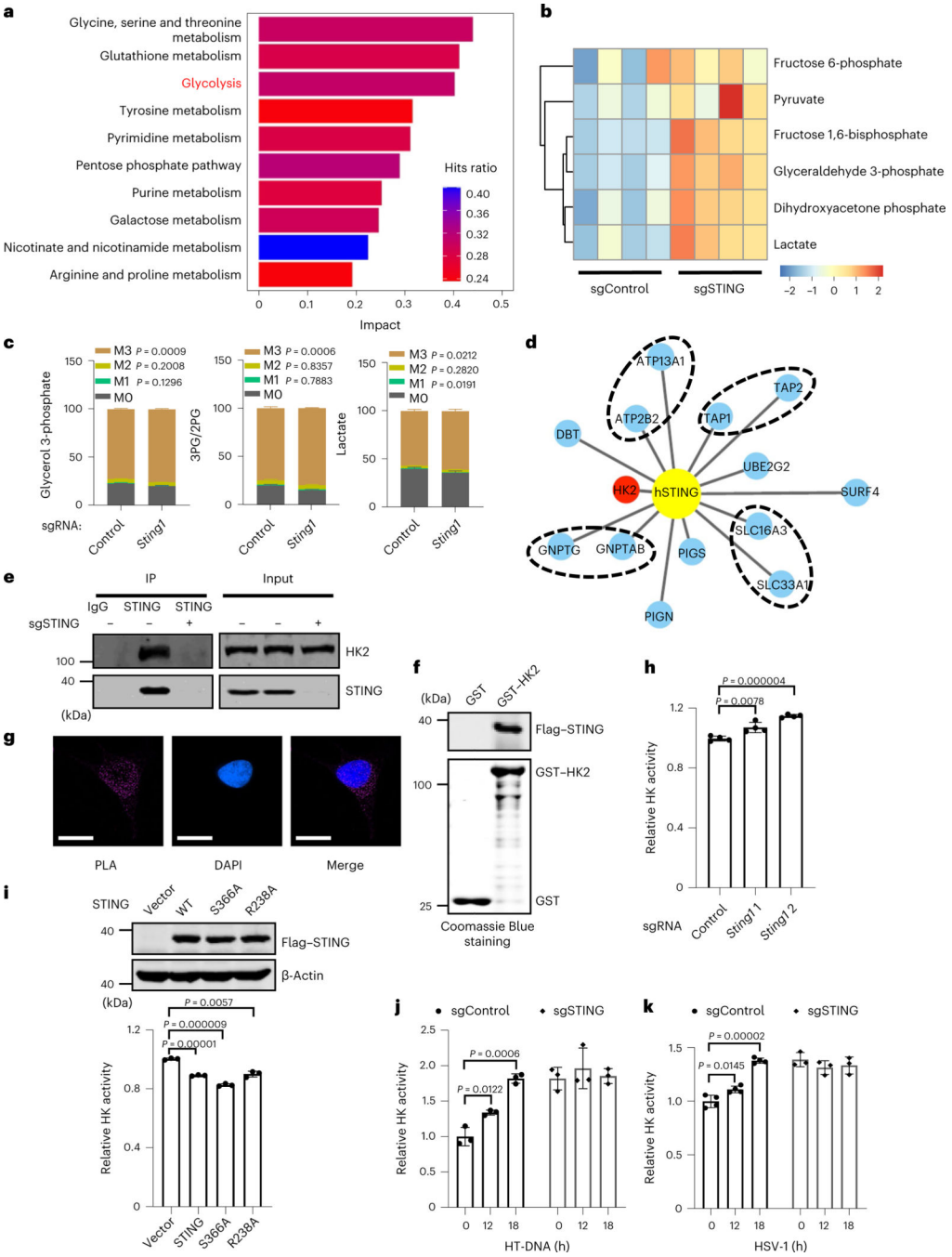

Fig. 3 |. STING restricts aerobic glycolysis by targeting HK2.

a,**b**, L929 cells were transduced with control sgRNA or sgRNA targeting *Sting1*, and the stable cells were collected for metabolomics analysis. The enrichment of the increased metabolic pathways (*Sting1* KO versus WT) (**a**) and a heat map of the metabolites in glycolysis (**b**) are shown. Data represent four biological replicates. **c**, [U-^{13}C] Glucose stable isotope tracer analyses were performed in control and *Sting1*$^{-/-}$ L929 cells. The M-labelled glycolysis intermediates (glycerol 3-phosphate, 3-phosphoglycerate/ 2-phosphoglycerate (3PG/2PG) and lactate) are shown. Four replicates were analysed for

each group. **d**, Flag–STING was immunoprecipitated from HEK293 cells stably expressing STING, and the binding of cellular proteins was analysed using mass spectrometry. **e**, Co-immunoprecipitation and immunoblot analysis of endogenous STING and HK2 in control and *STING1*$^{-/-}$ THP-1 cells. Anti-STING antibodies were used for immunoprecipitation. **f**, In vitro GST pull-down assay. GST or GST-HK2 purified from bacteria was used to pull-down Flag–STING affinity-purified from HEK293T cells. The binding fractions were analysed by immunoblotting, and purified GST and GST–HK2 were visualized by Coomassie Brilliant Blue staining. **g**, A PLA was performed to detect in situ STING–HK2 interaction. Scale bars, 10 μm. **h**, Analysis of HK activity in purified mitochondria isolated from control and *Sting1*$^{-/-}$ L929 cells. **i**, Measurement of mitochondrial HK activity in the reconstituted *Sting1*$^{-/-}$ L929 cells as indicated. **j**,**k**, Control and *Sting1*$^{-/-}$ L929 cells were stimulated with HT-DNA (**j**) or infected with HSV-1 (**k**), and mitochondrial HK activity was analysed. Data are mean ± s.d. of $n = 4$ (**h**), $n = 3$ (**i** and **j**) or $n = 4, 4, 4, 3, 3, 3$ (from left to right) (**k**) independent biological replicates. Statistical analysis was performed using two-tailed unpaired Student's *t*-tests. Data are representative of three independent experiments. Source numerical data and unprocessed blots are provided as Source Data.

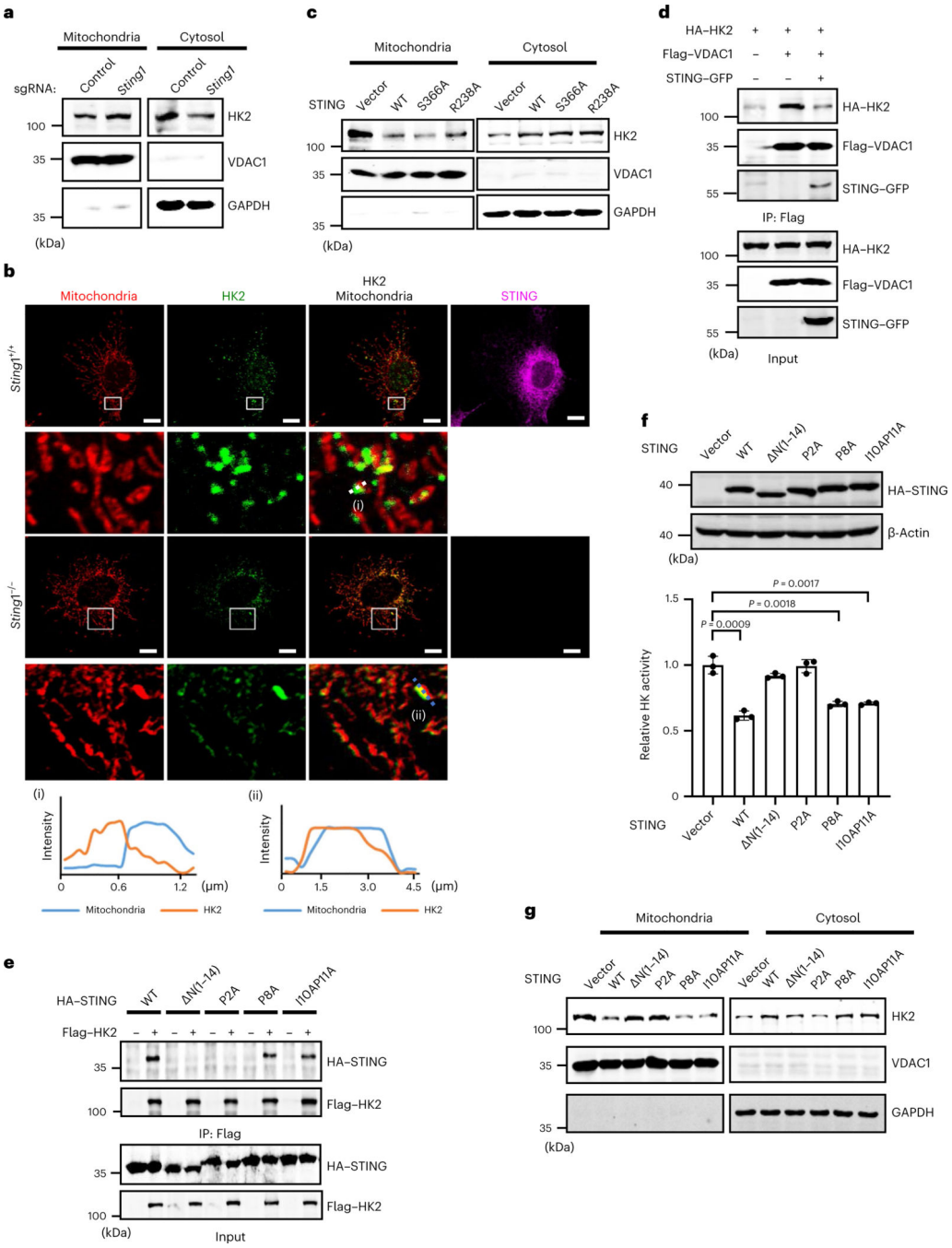

Fig. 4 |. STING inhibits HK2 mitochondrial localization to block its HK activity.

a, Mitochondrial and cytoplasmic fractions were isolated from control or *Sting1*$^{-/-}$ L929 cells and analysed using immunoblotting. **b**, Immunofluorescence staining of mouse lung fibroblasts (MLFs) derived from *Sting1*$^{+/+}$ and *Sting1*$^{-/-}$ mice. Scale bars, 10 μm. The areas indicated by boxes are magnified below. The fluorescence intensity profiles along the dotted lines (i and ii) are shown at the bottom. **c**, *Sting1*$^{-/-}$ L929 cells were reconstituted with vector control, WT STING or the indicated mutants. Mitochondrial and cytoplasmic fractions were isolated and analysed by immunoblotting. **d**, HEK293T cells

were transfected with the indicated plasmids, and WCLs were immunoprecipitated with anti-Flag agarose, followed by immunoblotting with the indicated antibodies. **e**, Flag–HK2 and HA-tagged STING or the indicated mutants were co-expressed in HEK293T cells. WCLs were immunoprecipitated with anti-Flag agarose and analysed by immunoblotting. **f**,**g**, Mitochondrial fractions were isolated from *Sting1*$^{-/-}$ L929 cells reconstituted with vector control, STING WT or the indicated mutants, and HK activity was measured (**f**). **g**, The mitochondrial and cytoplasmic fractions were analysed using immunoblotting. For **f**, data are mean ± s.d. of $n = 3$ indicated independent biological replicates. Statistical analysis was performed using two-tailed unpaired Student's *t*-tests. Data are representative of three independent experiments. Source numerical data and unprocessed blots are provided as Source Data.

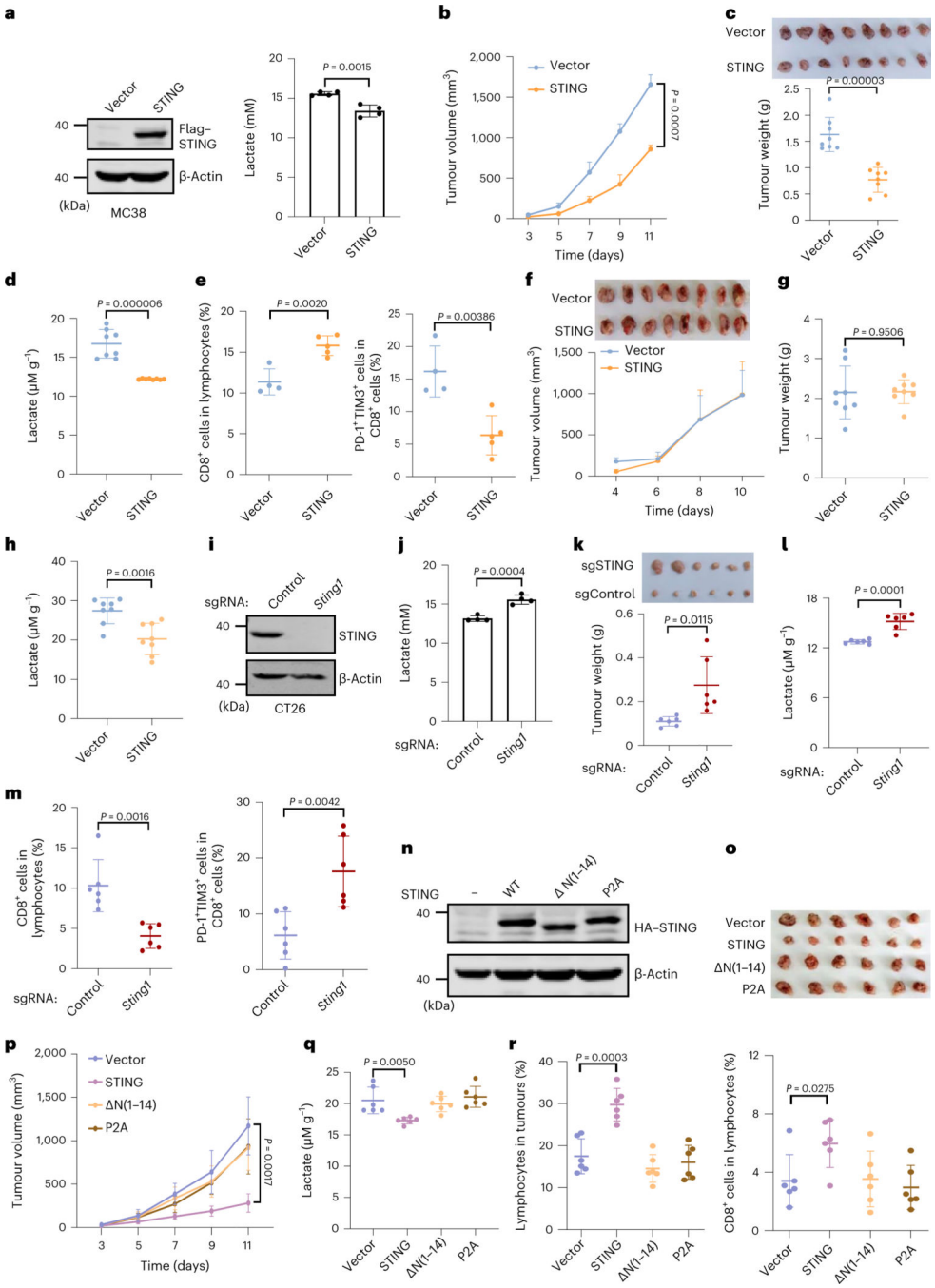

Fig. 5 |. STING restricts lactate production and promotes antitumour immunity in vivo.
a, MC38 cells were transduced with control (vector) lentivirus or lentivirus containing Flag–STING (left; representative of three independent experiments), and lactate production was measured (right). $n = 4$ biological repeats. **b**,**c**, MC38 cells as described in **a** were subcutaneously transplanted into C57BL/6J mice ($n = 8$ per group), the volume of tumours was quantified (**b**) and the size and weight of tumours are shown (**c**). **d**, Lactate levels in the tumours collected from **c** were measured. $n = 8$. **e**, MC38 cells as described in **a** were subcutaneously transplanted into C57BL/6J mice ($n = 4$ (vector group) and $n = 5$

(STING group)). Tumour-infiltrating $CD8^+$ T cells and the severely exhausted $CD8^+$ cells in tumours were analysed using flow cytometry. **f**–**h**, MC38 cells as described in **a** were subcutaneously transplanted into NSG mice ($n = 8$ per group). The tumour volume (**f**), weight (**g**) and lactate levels (**h**) were quantified. **i**, CT26 cells were transduced with control sgRNA or sgRNA targeting *Sting1* to generate KO cells. **j**, Measurement of the lactate levels in control or $Sting1^{-/-}$ CT26 cells. $n = 4$ biological repeats. **k**,**l**, CT26 cells as described in **i** were subcutaneously transplanted into BALB/c mice ($n = 6$ per group), the size and weight of tumours are presented (**k**) and lactate production in the tumours was measured (**l**). **m**, Flow cytometry analysis of the tumour-infiltrating $CD8^+$ T cells and the severely exhausted $CD8^+$ T cells isolated from CT26 tumour as described in **k**. $n = 6$. **n**–**p**, MC38 cells were transduced with control (vector) lentivirus or lentivirus containing STING or the indicated mutants. **n**, WCLs were analysed by immunoblotting. The cells were then subcutaneously transplanted into C57BL/6J mice ($n = 6$). Images (**o**) and quantification (**p**) of tumour size and volume are shown. **q**,**r**, Quantification of lactate production (**q**) and T cell infiltration (**r**) in MC38 tumours as described in **o**. $n = 6$. Data are mean ± s.d. Statistical analysis was performed using two-tailed unpaired Student's *t*-tests. Data are representative of three independent experiments. Source numerical data and unprocessed blots are provided as Source Data.

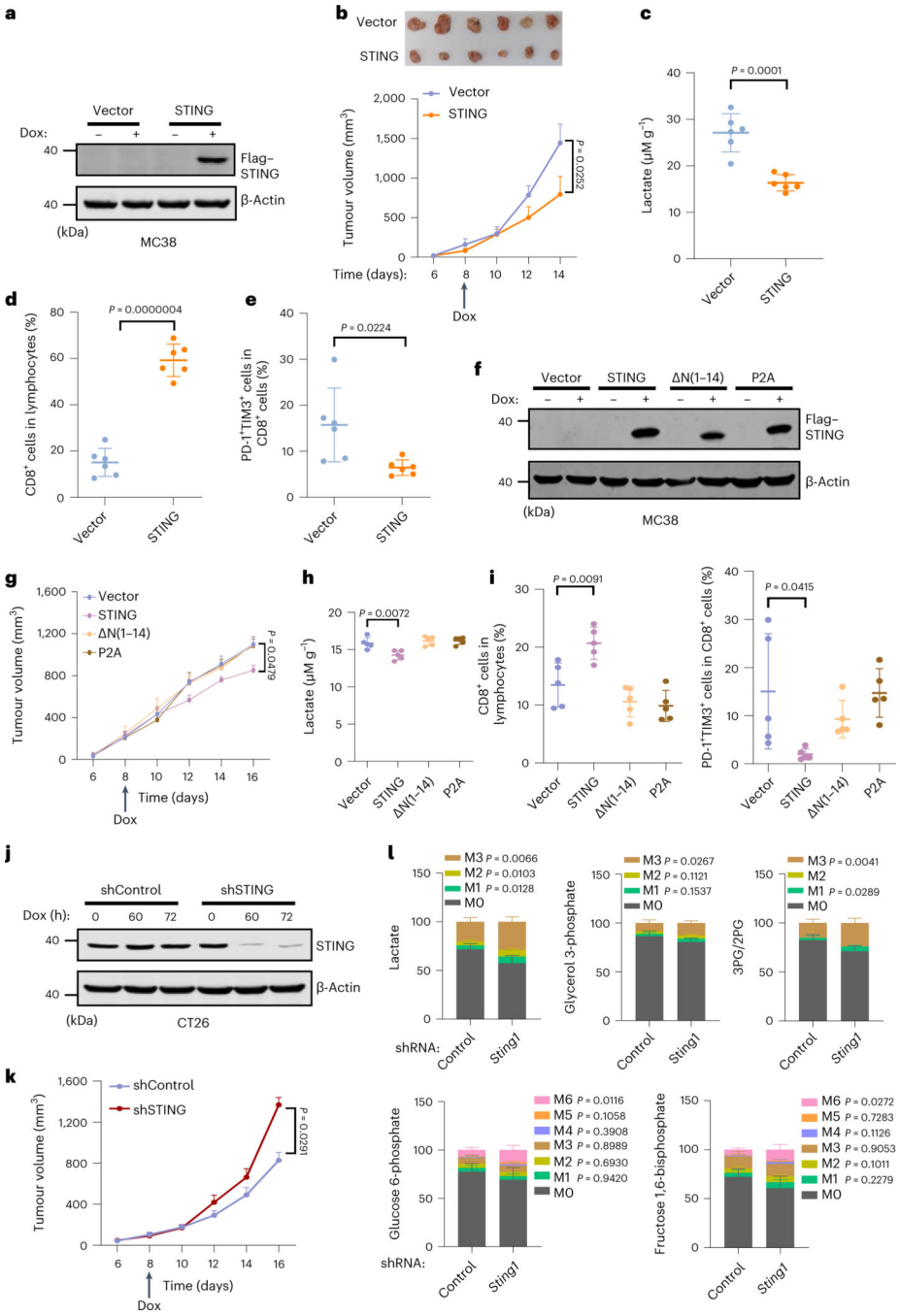

Fig. 6 |. STING restricts aerobic glycolysis in established tumours.

a, MC38 cells with doxycycline (Dox)-inducible expression of Flag–STING were cultured with or without doxycycline (500 ng ml^{-1}) for 24 h and then analysed using immunoblotting. **b**,**c**, MC38 cells as described in **a** were subcutaneously transplanted into C57BL/6J mice ($n = 6$). Doxycycline diet (200 mg kg^{-1}) was given when tumours were established on day 8 after implantation. The volume (**b**) and lactate levels (**c**) of tumours were quantified. **d**,**e**, Quantification of tumour-infiltrating $CD8^+$ T cells (**d**) and the severely exhausted $CD8^+$ cells (**e**) in tumours as described in **b**. $n = 6$. **f**, MC38 cells

with doxycycline-inducible expression of Flag–STING or the mutants were cultured with or without doxycycline (500 ng ml^{-1}) for 24 h and then analysed using immunoblotting. **g**,**h**, MC38 cells as described in **f** were subcutaneously transplanted into C57BL/6J mice ($n = 5$). Doxycycline diet (200 mg kg^{-1}) was given on day 8 after implantation, the volume of the tumours was quantified (**g**) and lactate levels in the tumours were measured (**h**). **i**, Quantification of tumour-infiltrating $CD8^+$ T cells in lymphocytes and the severely exhausted $CD8^+$ T cells in tumours as described in **g**. $n = 5$. **j**, CT26 cells stably expressing doxycycline-inducible control short hairpin RNA (shControl) or shRNA against *Sting1* were treated with or without doxycycline (500 ng ml^{-1}), and then analysed using immunoblotting. **k**, CT26 cells as described in **j** were subcutaneously transplanted into BALB/c mice ($n = 8$). Doxycycline diet (200 mg kg^{-1}) was given on day 8 after implantation, and the volume of tumours was quantified. **l**, CT26 cells as described in **j** were subcutaneously transplanted into BALB/c mice ($n = 6$ (control group) and $n = 7$ (STING group)). Doxycycline diet (200 mg kg^{-1}) was given on day 8 after implantation. In vivo [U-^{13}C]glucose stable isotope-labelling experiments were performed on day 16. The labelled glycolysis intermediates are displayed (M0–M6: mass isotopomers). Data are mean ± s.d. Statistical analysis was performed using two-tailed unpaired Student's *t*-tests. Data are representative of three independent experiments. Source numerical data and unprocessed blots are provided as Source Data.

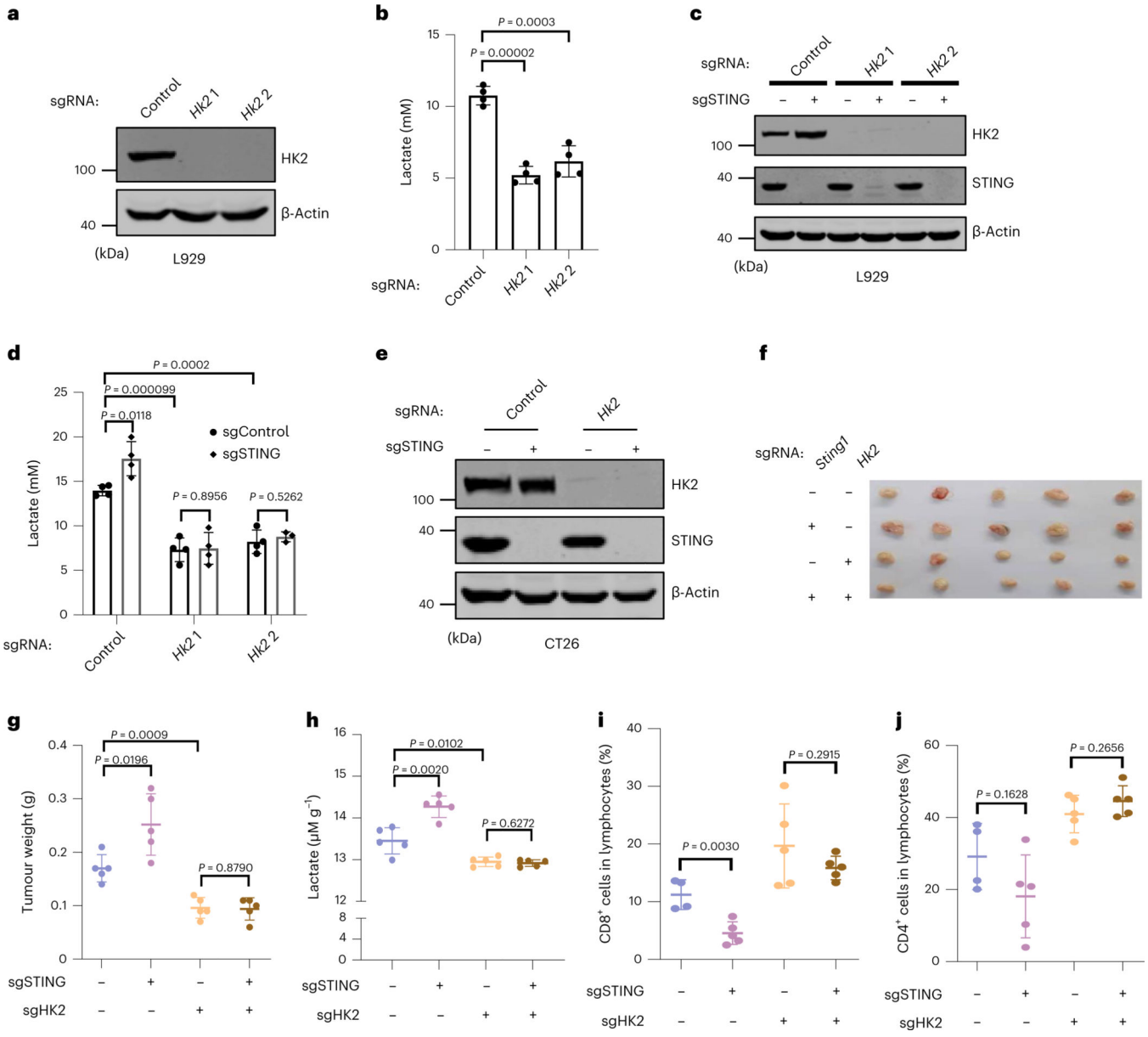

Fig. 7 |. HK2 is required for the cell-intrinsic tumour suppressor activity of STING.

a,**b**, L929 cells were transduced with control sgRNA or two sgRNAs targeting *Hk2*. WCLs were analysed using immunoblotting (**a**), and lactate production was measured (**b**). n = 4 biological replicates. **c**,**d**, L929 cells were transduced with control sgRNA or sgRNAs targeting *Hk2* and *Sting1* to generate KO cells. WCLs were analysed by immunoblotting (**c**), and lactate production was measured (**d**). From left to right, n = 4, 4, 4, 4, 4 and 3 biological replicates. **e**, CT26 cells were transduced with control sgRNA or sgRNA targeting *Hk2*, and the stable cells were further transduced with control sgRNA or sgSTING to generate double-KO cells. WCLs were analysed by immunoblotting with the indicated antibodies. **f**, CT26 cells as described in **e** were subcutaneously transplanted into BALB/c mice (n = 5 per group). The size of tumours at 15 days after transplantation is shown. **g**, The weight of tumours at 15 days after transplantation as described in **f**. n = 5 per group. **h**,

Lactate production in the CT26 tumour as described in **f** was measured at 15 days after transplantation. $n = 5$. **i**,**j**, CT26 cells as described in **e** were subcutaneously transplanted into BALB/c mice ($n = 4$ (control group) and $n = 5$ (other groups)). The intratumoural infiltration of $CD8^+$ (**i**) and $CD4^+$ (**j**) T cells was detected. Data are mean ± s.d. Statistical analysis was performed using two-tailed unpaired Student's *t*-tests. Data are representative of three independent experiments. Source numerical data and unprocessed blots are provided as Source DatamRuby3-mSTING .

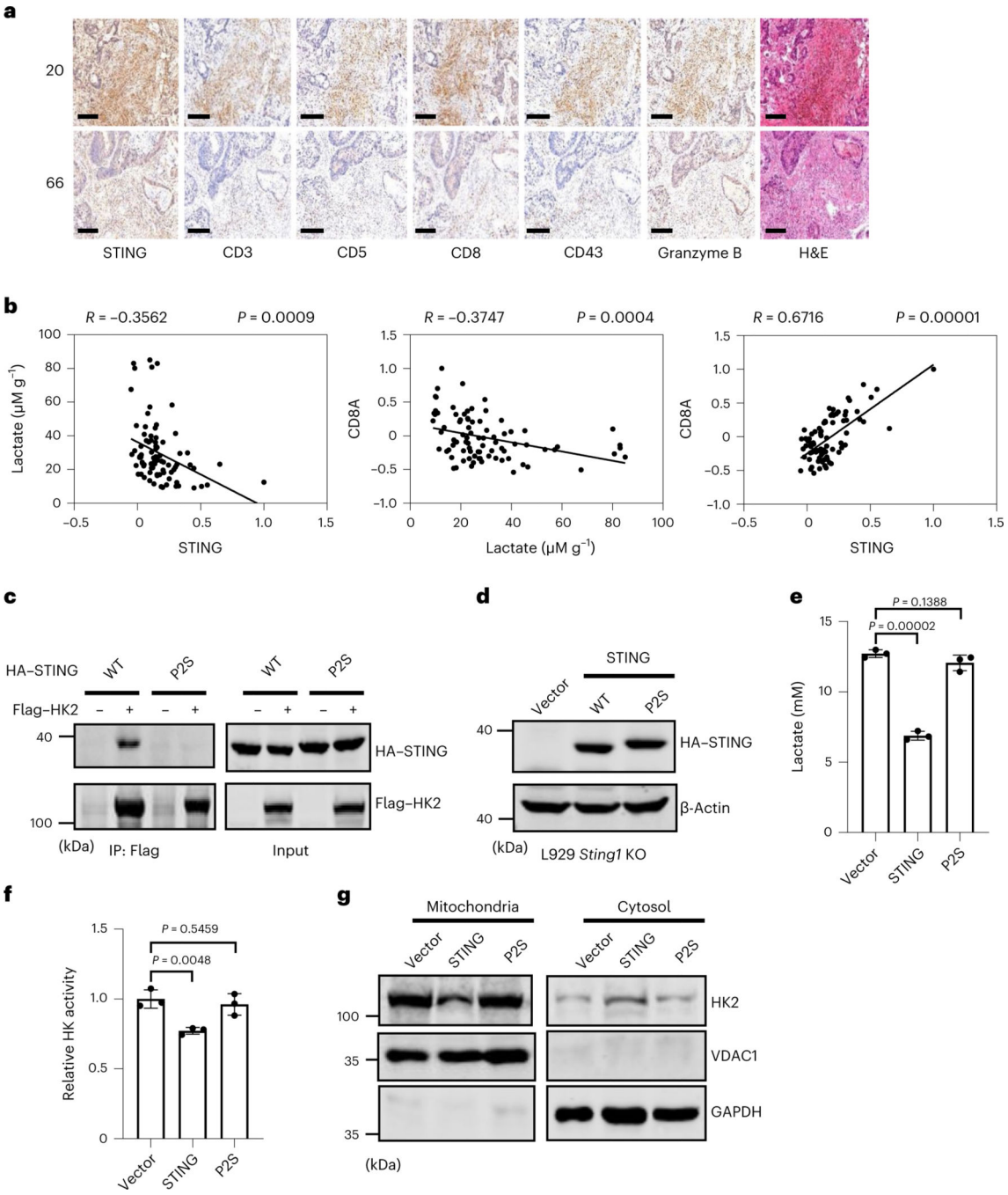

Fig. 8 |. Lactate levels in human colorectal carcinomas negatively correlate with STING expression and antitumour immunity and a naturally occurring STING(P2S) SNV loses the ability to restrict HK2 and glycolysis.

a, Representative IHC and H&E staining of tumour tissue in human colorectal carcinomas, showing lymphocyte cell infiltration and pathology. Scale bars, 200 μm. **b**, Correlations between the lactate levels, STING expression and CD8A expression in colorectal tumour tissue. $n = 84$. **c**, HEK293T cells were transfected with the indicated plasmids, and WCLs were immunoprecipitated with anti-Flag agarose. Precipitated proteins and WCLs were analysed by immunoblotting with the indicated antibodies. **d**,**e**, *Sting1*$^{-/-}$ L929

cells were reconstituted with vector control, WT STING or the STING(P2S) mutant. WCLs were analysed using immunoblotting (**d**), and lactate production was measured (**e**). $n = 3$ biological replicates. **f**,**g**, Mitochondrial and cytoplasmic fractions were isolated from the reconstituted cells as described in **d**, HK activity was measured (**f**) ($n = 3$ biological replicates) and the mitochondrial and cytoplasmic fractions were analysed using immunoblotting (**g**). Data are mean ± s.d. Statistical analysis was performed using two-tailed unpaired Student's *t*-tests (**e** and **f**) and two-sided Pearson's χ^2 tests (**b**). Data are representative of three independent experiments. Source numerical data and unprocessed blots are provided as Source Data.